UNIVERSITY of LIMERICK

OLLSCOIL LUIMNIGH

Theoretical Investigation of the Effect of Subtle Structural Dynamics on CO_2 sorption in TIFSIX-3-Ni, a Hybrid Ultramicroporous Material (HUM)

by

Meagan Mulcair

Department of Chemical Sciences

and

Bernal Institute

Supervisors

Prof. Michael J. Zaworotko

Department of Chemical Sciences

Bernal Institute, University of Limerick

Dr. Syed A.M. Tofail

Department of Physics and Energy

Materials and Surface Science Institute, University of Limerick

A thesis submitted in fulfilment of the requirements for the degree of Masters of Science by Research

Submitted to the University of Limerick, October 2017

Abstract

The release of carbon dioxide (CO_2) emissions into the atmosphere is a leading contributor to global warming. Carbon capture and sequestration (CCS) strives to mitigate the effects of CO_2 on the atmosphere, traditionally by expensive and energy-intensive chemisorptive approaches. CO_2 capture by physisorbents such as hybrid ultramicroporous materials (HUMs) is a step toward cheaper and more efficient CCS. In this study, the effect of pyrazine ring orientation upon CO_2 adsorption is investigated for **TIFSIX-3-Ni,** a leading HUM for CO_2 selectivity. Rigid systems are constructed by eliminating disorder from the unit cell as determined by *in situ* characterization. Density Functional Theory (DFT) and Grand Canonical Monte Carlo (GCMC) methods are used to investigate the effect of tilting and ordering pyrazine rings upon CO_2 loading and isosteric heat of adsorption (Q_{st}). Results show that more edge to face interactions between pyrazine CH moieties and the CO_2 molecule induce a preferred binding site. Systems with chemically distinct binding sites exhibit a Q_{st} trend comparable to that which is experimentally observed, showing first preference for binding in smaller pores using models treated with both UFF and OPLS-AA Lennard-Jones parameters. It is also noted that the degree of pyrazine ring tilting affects the energetics of the sorbent-sorbate interactions, meriting further study. This work highlights the importance of subtle structural dynamics in adsorption performance of leading porous materials, and can be used to guide further fine-tuning of physisorbent materials for gas sorption applications.

Declaration

"I, Meagan Mulcair, hereby declare that this thesis is entirely my own work and has not been submitted to any other university or higher education institute, nor for any academic award in this university. Where use has been made of the work of other people, it has been fully acknowledged and/or referenced."

…….. …….

Acknowledgements

I would like to express sincere gratitude to my supervisor, Prof. Michael Zaworotko for his support and guidance throughout my Masters studies and graduate research experience at University of Limerick. It has been an honour to be a member of the Crystal Engineering Group at UL, and a learning experience I will carry with me throughout the course of my career.

I would also like to acknowledge my co-supervisor, Dr. Syed Tofail, for his advice. Thank you to Dr. Damien Thompson and his research group (University of Limerick) for help and advice over the course of my studies at UL.

My most sincere thanks to Prof. Brian Space (University of South Florida) for his guidance, support and hospitality throughout the course of my research experience at both UL and USF. It has been a joy to collaborate with and learn from his group at USF. Your support and your friendship has truly been a highlight of my graduate experience thus far.

A special thank you to Dr. Drahomir Chovan (UL) and to Adam Hogan (USF) for their continuous support and guidance, without whom this project would have been impossible. I am grateful both for your knowledge and friendship alike.

Thanks to the Crystal Engineering group at UL for imparting with me some of their vast knowledge of porous materials, crystal engineering, gas sorption and indeed many cultures along the way. Especial thanks to Dr. David Madden, Dr. Carol Hua,

Dr. John Perry IV, Daniel O'Nolan and Amrit Kumar for working directly with me on this project. Thank you also to Dr. Alankriti Bajpai, whose artistic presentation skills will forever be an aspiration to reach.

I am grateful to the Bernal Institute, the Materials and Surface Science Institute and to the Department of Chemical Sciences for an outstanding working environment and endless support and resources. Thank you also to Maria Munroe and to the members of Dr. Kevin Ryan's group (UL) for their help in lab demonstration and their friendship alike.

Thank you to the Irish Centre for High End Computing (ICHEC) and to XSEDE for the computational resources used throughout the course of this work. Thank you also to the Science Foundation Ireland (SFI) for the financial support of this project.

Last but not least, thank you to my family and friends for your endless support and compassion over the course of my time at UL. Your love and encouragement mean the world to me. Thank you.

Table of Contents

List of Figures

List of Tables

List of Publications

1. **Meagan Mulcair**, Daniel O'Nolan, Adam Hogan, Drahomir Chovan, Carol Hua, Amrit Kumar, Syed A.M. Tofail, Brian Space, David G. Madden and Michael J. Zaworotko, "*Insight into CO_2 sorption in TIFSIX-3-Ni Obtained by in situ Synchrotron Structural Characterization and Molecular Simulations*", Journal of the American Chemical Society, Communication under review, October 2017 (See **Appendix**)

2. **Meagan Mulcair**, Syed A.M. Tofail and Michael J. Zaworotko, *"Effect of Pyrazine Ring Tilting upon CO_2 Adsorption in TIFSIX-3-Ni, a Hybrid Ultramicroporous Material*", 100th Canadian Society of Chemistry Exhibition (CSC), Materials Science Division, Toronto, Canada, May 2016 (Poster Presentation)

3. **Meagan Mulcair**, Daniel O'Nolan, Adam Hogan, Drahomir Chovan, Syed A.M. Tofail and Michael J. Zaworotko, "*Molecular Modelling of Porous Materials*", C.E.L.T.I.C., Killarney, Ireland, March 2016 (Oral Presentation)

Chapter 1: Introduction

The emission of carbon dioxide into the atmosphere is one of the leading contributors to global climate change and is largely a direct consequence of anthropogenic activity.[1, 2] These emissions are released into the atmosphere through the burning of fossil fuels and industrial processes, and act as an insulator, impeding the escape of radiation from the atmosphere. With no foreseeable alternative to fossil fuels as the leading energy source in the near future, it is imperative to prioritise mitigation of the effects of carbon dioxide on the atmosphere. This can be achieved by carbon capture and sequestration (CCS).[3, 4] CO_2 removal is also important from an industrial perspective for processes such as upgrading of biogas and syngas, and natural gas sweetening.[5, 6] Therefore, the potential to store, separate and reuse carbon dioxide has led to much research interest in the design of new materials for CCS. Current CO_2 removal strategies are heavily dependent upon energy intensive chemisorption based technologies such as liquid amine absorption. These chemisorption based technologies suffer from significant issues such as corrosion, amine loss which makes them expensive and inefficient to operate.[7-9]

Physisorption based gas separation technologies potentially offer a cheaper and more efficient alternative for both bulk and trace carbon capture. Metal-Organic Materials, (MOMs),[10] are a promising class of porous crystalline materials with respect to gas adsorption applications, combining high porosity, high surface area[11] and functionalisation[12, 13] through the metal moiety and organic ligands to optimise

specific adsorbent/adsorbate interactions. Subclasses of MOMs include Porous Coordination Polymers[14, 15] and Metal-Organic Frameworks[16-19] which are especially promising for gas separation and storage by physisorption as they exhibit permanent porosity. The reticular design strategy enables precise control over the pore size and pore chemistry of these MOMs.[20] This strategy relies on the exploitation of molecular building blocks (MBBs)[10, 20, 21], which are metal clusters or rigid molecular complexes which are linked together with organic linkers Due to this inherent modularity,[22, 23] structure-property relationships are amenable to fine-tuning. In conjunction with the ability to reasonably predict a material's overall topology, this allows not only post-synthetic modification but also rational design by pre-synthetic modification, i.e. by applying a crystal engineering strategy.[24]

Crystal engineering is especially amenable to the design and synthesis of novel MOMs for gas sorption application as it lends itself to exquisite control over pore size and pore chemistry. By this strategy, MOMs can be designed and synthesised through a systematic and application specific approach provided the crystal packing and pore chemistry is both predicted and understood.[10] Through a crystal engineering approach, a new subclass of crystalline porous materials has been developed, called hybrid ultramicroporous materials (HUMs).[24-26] These materials are distinguishable from traditional MOFs due to the presence of inorganic hexafluorometallate anions which pillars 2D square grid (**sql**) coordination networks to form 3D materials with primitive cubic (**pcu**) topology and ultramicroporous (>7Å)

pore networks. This ultramicropore together with the electronegative inorganic pillar, enhances the interactions between the adsorbent and small polarisable adsorbate molecules such as CO_2.[25] The parent material of this platform is **SIFSIX-1-Zn,** $[Zn(4,4'\text{-bypyridine})_2(SiF_6)]_n$, which was first reported in 1995.[27] This led to the development of the prototypal HUM, **SIFSIX-3-Zn.**[22, 28] To date, the development of such materials has led to benchmark performance with respect to environmentally and industrially important gas separations including the separation of acetylene and ethylene, carbon dioxide and nitrogen and methane, and noble gas separations such as Xenon and Krypton[22, 29-37]. Furthermore, HUMs have shown potential in the direct air capture of CO_2 and in water vapour capture.[38]

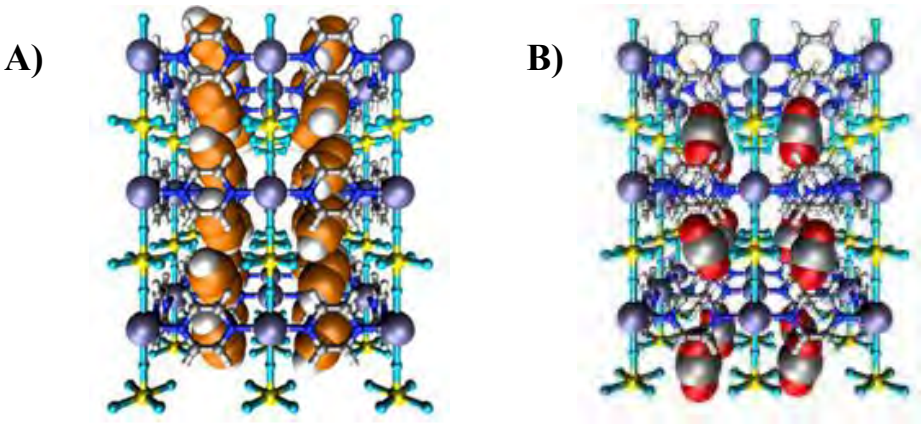

Figure 1: Illustration of the binding sites of a) C_2H_2 (orange and white) and b) CO_2 molecules (red and grey) in **SIFSIX-3-Ni**, a hybrid ultramicroporous material with exceptional CO_2/C_2H_2 selectivity at low partial pressures. Images taken from reference 30.[30]

A recently reported variant of the **MFSIX-L-M'** HUM platform, **TIFSIX-3-Ni,** ($[Ni(pyrazine)_2(TiF_6)]_n$),[39] has been shown to surpass current benchmark HUM

physisorbents such as **SIFSIX-3-Ni** with respect to the isosteric heat of adsorption (Q_{st}) of CO_2. Isostructural to previously reported compounds of the **MFSIX-3-M'** family, **TIFSIX-3-Ni** is comprised of octahedral Ni^{2+} nodes which are coordinated by pyrazine linkers in equatorial positions yielding $Ni(pyrazine)_2$ square grids, as determined by *in situ* synchrotron powder X-ray diffraction (PXRD). These grids are pillared by TiF_6^{2-} anions to form the resulting ultramicroporous primitive cubic topology, **pcu,** coordination network.

A single binding site was located for CO_2 in **TIFSIX-3-Ni**.[29] This was expected as the structure of this material is analogous to that of materials such as **SIFSIX-3-Ni** and **SIFSIX-3-Cu**. A tight binding site is afforded by unit cell parameters of $a = b = 6.99784(14)$ Å and $c = 7.79358(18)$ Å, which is compatible with the experimentally observed, high Q_{st}. Substitution of the SiF_6^{2-} moiety with a Ti-based analogy affords longer equatorial Ti···F bonds (1.61 Å vs. 1.87 Å M···F bond distance, respectively) and subsequently, shorter axial Ti···Ni bonds and smaller *a*- and *b*- cell axes. As a result, this leads to both a smaller unit cell and tighter CO_2 binding site than is present in the SiF_6^{2-} equivalent (Figure 2).

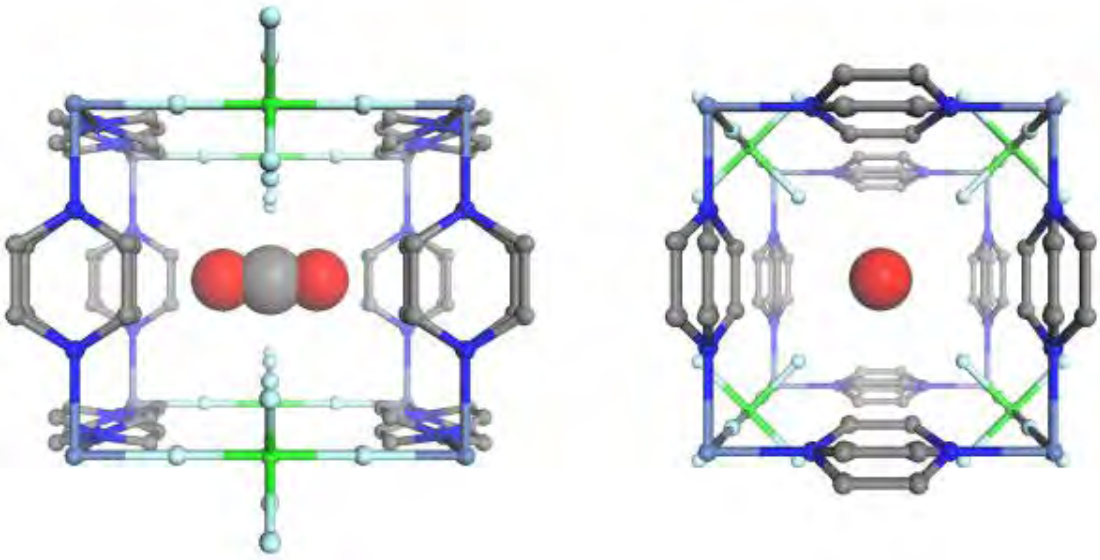

Figure 2: Illustrations of the CO_2 binding site in **TIFSIX-3-Ni**.

The Q_{st} reported for CO_2 in **TIFSIX-3-Ni** greatly exceeds those reported for classic physisorbent materials such as **HKUST-1**, **Mg-MOF-74**, **Zeolite 13X** and **UiO-66-NH2**.[39] Furthermore, the experimental Q_{st} trend is atypical for **TIFSIX-3-Ni**, increasing upon initial loading from (0.1 to 0.6 mmol g^{-1}) in contrast to the typical decreasing trend which is observed for other materials.[39] This increase suggests potential cooperative sorption of CO_2 molecules whereby the adsorption of one guest molecule is enhanced by the adsorption of one prior. This possibility is practically relevant as loading does not affect the selectivity of the adsorbent-adsorbate interaction. Such an occurrence is also scientifically relevant in that an explanation as to why this trend might occur would aid understanding of this class of materials thus enabling more targeted design and synthesis for future generations.

Although determined as having equivalent unit cell parameters to **NbOFFIVE-1-Ni**,[34] an isostructural fluoro-oxy pillared ($NbOF_5^{2-}$) HUM by *in situ* synchrotron PXRD, **TIFSIX-3-Ni** was revealed to display less pronounced ring tilting, allowing for a larger pore aperture which is conducive to superior CO_2 adsorption kinetics. The pyrazine rings were determined to be crystallographically disordered over two sites at both zero and full loading of CO_2 in **TIFSIX-3-Ni**. Between these extremes, data collection was impeded by experimental limitations. Due to the ultramicroporous pore size of the binding site in **TIFSIX-3-Ni**, subtle structural dynamics such as the orientation of the pyrazine rings could potentially have a significant effect on the adsorption equilibrium and kinetics. This could lead to an explanation for the initially rising Q_{st} trend as observed by experiment, lending valuable insight into the sorption performance and loading mechanism of these benchmark materials.

Research Hypothesis

Through a combination of DFT and GCMC simulation, subtle structural variations, the location of binding sites, energetics of adsorbent-adsorbate interactions and charge distribution as well as trends in gas sorption isotherms and isosteric heat of adsorption are frequently successfully carried out and compared with experiment. Using these techniques in the analysis of the **SIFSIX-3-M'** materials, it has been

shown that smaller metal ions lead to smaller pores and greater binding energy, with a CO_2 Q_{st} trend of M' = Cu > Ni > Zn.[40] In the same study, it was deduced by molecular modelling that a 45° angle of the equatorial F-atoms relative to the *c*-axis proved optimal for CO_2 selectivity in these pores. Computational studies have also illustrated the effects of co-adsorption on Q_{st} and the effects of replacing the **SIFSIX** moiety with **TIFSIX**, as mentioned above.[41] Overall, through extensive computational studies, it is clear that with regard to the **MFSIX-3-M'** family of HUMs, the current benchmarks for CO_2 selectivity share a tight binding pore of < 4 Å, highly electronegative equatorial F-atoms at a 45° angle binding to a single CO_2 fixing it in place at the center of each cell, and induced polarisation of the CO_2 upon adsorption. Recently, the Xe/Kr performance of **SIFSIX-3-Ni** and an analogous variant, **SIFSIX-3-Fe**, was compared by similar computational methods.[42] An inflection was observed in the Xe isotherm of **SIFSIX-3-Ni** but not in **SIFSIX-3-Fe**, in spite of their physical and chemical similarities as materials. Upon further computational investigation, it was observed that the pyrazine linkers in each of these materials were free to rotate ±16°.[42] Such ring rotation/ordering has also been previously reported for **SIFSIX-1-Cu** in another computational study.

The recently reported **TIFSIX-3-Ni** which exhibits benchmark performance in terms of CO_2 selectivity is analogous in structure to **SIFSIX-3-Ni**, and exhibits an unusual increasing Q_{st} trend at low loading before later decreasing.[29] This rise in Q_{st} was also observed for **NbOFFIVE-1-Ni**, for which ring rotation and ring orientation

is also suspected to be an important contributor to the favourable Q_{st} trend. For these reasons, it was hypothesised that a similarly subtle structural variation in **TIFSIX-3-Ni** could drastically alter the binding site interactions with CO_2. Should the rings order to optimise adsorbent-adsorbate interactions upon binding, a more global effect of ring rotation and orientation could be induced. This indicates a potential mechanism for the kinetic co-adsorption of CO_2 molecules as suggested by the experimental Q_{st} trend until approximately half loading of the material. At this point, few if any preferable sites would remain if a suitable energy difference between sites of different ring configurations was present. As a result, this study herein aims to analyse the effects of both the degree of ring tilting and the orientation of pyrazine rings about the CO_2 binding site in **TIFSIX-3-Ni**. This analysis aims to provide a means of potentially explaining the Q_{st} trend observed experimentally, and better understanding the behaviour of HUMs to guide their development for gas sorption applications.[43]

Chapter 2: Literature Review

2.1 Introduction

Metal-Organic Materials, (MOMs),[10] have attracted much research interest due to their highly porous nature and their large surface area.[10, 44-46] These materials share a common composition of metal centres (nodes) and organic linkers and are extended structures in 1-D, 2-D and 3-D.[10]. By carefully choosing the node and spacer combination, the resulting MOM topology can be designed to dictate the pore size and pore chemistry of the material. As a result of manipulating this inherent modularity, these materials have been used in a broad range of applications such as catalysis,[47] ion-exchange, non-linear optics, magnetism, luminescence and drug delivery.[15, 48] Porous Coordination Polymers, (PCPs),[14] and Metal-Organic Frameworks, (MOFs),[16] are subclasses of MOMs which exhibit permanent porosity. They have thus proven especially promising in the area of gas separation and gas storage.[48, 49] Materials in this field such as **MOF-5**[43, 50], **HKUST-1**[51]and **Mg-MOF-74**[52] share the characteristics of permanent porosity and a large surface area. Porous materials are classed and categorised in accordance with their pore size. *Macroporous* materials exhibit the largest pores, exceeding 50nm. *Mesoporous* materials present a pore size in the range of 2nm-50nm. *Microporous* materials have a pore size smaller than 2 nm. The final classification is for the materials with a pore size of less than 7 Å, namely *Ultramicroporous* materials.

2.1.1 Hybrid Ultramicroporous Materials (HUMs)

A recently defined subclass of MOMs has emerged in which the strategy for optimising adsorbent-adsorbate interactions focuses on pre-synthetic control and modification of the pore size and pore chemistry. Hybrid ultramicroporous materials (HUMs) have developed as a result of exploitation of the modular nature of MOMs using a crystal engineering approach [24-26] HUMs have been found to exhibit benchmark performance across a wide range of gas separations.[22, 29-33, 42] These materials comprise of a tight ultramicropore and anionic, electronegative pore chemistry, which give way to their outstanding performance in terms of their selectivity towards small polarisable gas adsorbates.[25]

HUMs are currently based on three platforms. The first platform is the **MFSIX-L-M'** platform, of which the parent material was first reported in 1995.[27] These materials comprise of transition metal nodes, **M'** (e.g. Zn^{2+}, Cu^{2+}, Ni^{2+}, Co^{2+}), which pillar square grid (**sql** topology) via pyridyl organic ligands, **L** (e.g. pyridine, bipyacetelene), and hexafluorometalate anions, **MFSIX** (e.g. SiF_6^{2-}, TiF_6^{2-}).[25] The second topology, **mmo**,[53-55] shares the similarity of square grids based on transition metals, but these self-catenated neutral nets $[M(L)_2]$ differ from the **MFSIX-L-M'** platform in that they are angularly pillared with chromate (CrO_4^{2-}), molybdate (MoO_4^{2-}), or tungstate (WO_4^{2-}) inorganic pillars. The HUM platform **DICRO-X-M**, where dichromate pillars (**DICRO**), ligands (**X**) and transition metals (**M** = Fe^{2+}, Co^{2+}, Ni^{2+}, Cu^{2+}) form primitive cubic lattice structures.[25] **NbOFFIVE-1-Ni** is a member of the

new HUM platform, **MO_xF_{6-x}-L-M**, in which square-grid layers of Ni^{2+} and pyrazine bridge with $NbOF_5^{2-}$ pillars to construct a 3D HUM with fluoride anions enclosed in square-shaped channels.[34] **AlFFIVE-1-Ni** is a material of another recently reported HUM platform, **$MF_5.H_2O$-L-M**, in which the contracted square-channels enclose a periodic array of fluorine moieties and open metal sites.[38] For the purpose of this study, this review will focus on members of the **MFSIX-L-M'** platform.

The prototypal **MFSIX-L-M'** platform was first published in 1995, as $[Zn(4,4'\text{-bypyridine})_2(SiF6)]_n$, later known as **SIFSIX-1-Zn**,[27] where **SIFSIX** represents the SiF_6^{2-} anion, **1** represents the bipyridine linker (or bpy) and Zn represents the metal moiety, Zn^{2+}. This material was the first of its kind, guiding the development of the **MFSIX** family. Comprising of cationic square grids and linear bifunctional anionic ligands, **SIFSIX-1-Zn** shares the permanent porosity and susceptibility to fine-tuning as do later synthesised **MFSIX** materials. The effective pore size however, being 8 x 8 Å, is beyond the criteria for an ultramicropore, bearing more similarity to the pore size of large zeolites than with later designed HUMs.[27] This key feature of a small pore size was later recognised to be of utmost importance in the effectivity of HUMs in terms of optimising adsorbent/adsorbate interactions.[25, 56]

Another material of the **SIFSIX** platform which exhibits a larger pore size, 13.05 Å, is **SIFSIX-2-Cu**.[22, 41] This material differs from **SIFSIX-1-Zn** in the choice of both linker, bipyridine (or "bpy") and metal moiety, Cu^{2+}. Although this

material has a large surface area, the CO_2 sorption performance is low with a selectivity of only 22 kJ mol^{-1} as the pore size remains larger than that of an ultramicropore, meaning that the CO_2 binding site is effectively not as tight. In spite of this, **SIFSIX-2-Cu** could offer potential in the area of gas storage as, while the selectivity is reasonably poor, the large surface area makes it a good candidate with respect to other MOMs.[41] The interpenetrated polymorph of this material, **SIFSIX-2-Cu-i**, where **i** represents a mode of interpenetration, shows much improved selectivity toward CO_2.[41, 57] While the surface area of this material is lower (735 m^2 g^{-1}), a pore size of 5.15 Å ensures the tight, ultramicroporous pore which leads to favourable CO_2 binding energies, in this case, 31.9 kJ mol^{-1}.

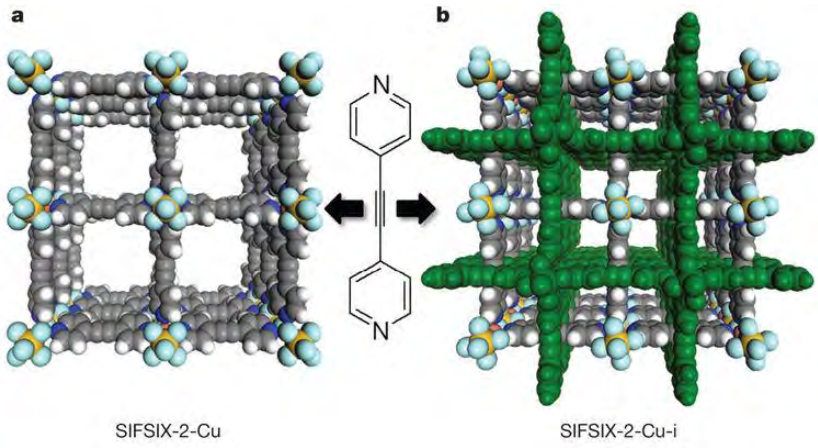

Figure 3: SIFSIX-2-Cu and **SIFSIX-2-Cu-i**. Colour code: C (grey), N (blue), Si (yellow), F (light blue), H (white). All guest molecules are omitted for clarity. Note that the green net represents the interpenetrated net in **SIFSIX-2-Cu-i**. The nitrogen-containing linker present in **SIFSIX-2-Cu** and **SIFSIX-2-Cu-i** is 4,4′-dipyridylacetylene (dpa). Image taken from reference number 22 [22]

A recently reported material with a slightly longer linker, azobipyridine, **SIFSIX-14-Cu-i**, undergoes phase transformation in the presence of water.[58] While this material is analogous to **SIFSIX-2-Cu-i**, studies on water sorption in these materials indicate that the longer and more hydrophilic nature of the linker plays a significant role in water sorption performance and in phase transformation.[58] These results further highlight the role of importance played by subtle structural variations in materials at the ultramicroporous level in both maintaining the structural integrity of the material and in the strength of binding interactions.

Another interesting feature of **SIFSIX-2-Cu-i**, which was reported following computational studies on CO_2 sorption, indicates that co-adsorption plays a role in the mechanics of how CO_2 loads in this material. Favourable vertical-horizontal configurations of CO_2 were elucidated in the structure computationally, essentially resulting in a T-shape trend of CO_2 molecules along the channels upon full loading.[30] This loading trend results in an increasing Q_{st} trend suggesting CO_2 co-adsorption. This feature makes **SIFSIX-2-Cu-i** a good candidate for interesting diffusive kinetic studies in the future.[41] Co-adsorption trends were also reported in a material analogous to **SIFSIX-1-Zn** with a Cu^{2+} metal moiety substitution, **SIFSIX-1-Cu**. In this material it was observed that upon full loading, CO_2 molecules align with a slipped parallel configuration along the channels.[41] The additional adsorbate-adsorbate interactions as a result of such an alignment would have a favourable effect on the CO_2 isosteric heat of adsorption (Q_{st}). Having a larger surface area but also a

larger pore size (9.54 Å) relative to **SIFSIX-2-Cu-i**, energetics for CO_2 sorption in the **SIFSIX-1-Cu** binding site are reported as 26.5 kJ mol^{-1}. This is less favourable to that determined for **SIFSIX-2-Cu-i**, indicating greater importance of pore size in HUM adsorbent-adsorbate interactions relative to the importance of large surface area.

Similar to **SIFSIX-1-Zn**, **SIFSIX-1-Cu** comprises of a flexible bipyridine linker in which the rings are free to rotate in the absence of a guest molecule.[59] Like **SIFSIX-14-Cu-i**, this material decomposes at low water uptake, supporting the idea that a large pore is more susceptible to hydrolysis.[58] Computational studies also revealed that the entire F···Si···F fork, rather than the isolated F atoms, in **SIFSIX** materials like **SIFSIX-1-Cu** directs the sorption of CO_2 and gradual ring ordering was reported for **SIFSIX-1-Cu** in earlier studies.[60] These features further indicate the importance of subtle structural variations in the sorption performance of these highly charged materials of permanent porosity when considering such tight potential binding sites and narrow pores.

2.1.2 CO_2 Adsorption: SIFSIX-3-M' Materials

Perhaps the greatest success thus far concerning the gas sorption and separation performance of the **SIFSIX** variants of the **MFSIX** family has been the substitution of bipyridine and bipyacetalene linkers with the much smaller pyrazine linker (pyz) to create **SIFSIX-3-M**' materials[22, 36, 61] which exhibit benchmark

CO_2 sorption and separation performance.[22, 30, 39] Comparing **SIFSIX-1-Cu** with **SIFSIX-3-Cu**,[36] the effect of shortening the organic linker dictates a much smaller pore size (3.54 Å), much smaller surface area (300 $m^2 g^{-1}$) and a dramatically increased CO_2 binding energy of 54 kJ mol^{-1}.[36, 41, 61] **SIFSIX-3-Cu** exhibits only one type of CO_2 sorption in comparison to the slipped parallel configuration observed in its bipyridine counterpart, **SIFSIX-1-Cu**, where the CO_2 molecule is fixed at the centre of the cell.[41] However, although **SIFSIX-3-Cu** is highly unstable, the higher CO_2 binding energy is indicative of smaller pore size leading to significantly favourable binding energetics.[40] The singular binding site of CO_2 at the center of the site essentially fixed in place by the C···F interactions as a result of the F···Si···F forks confirms that there is a much larger electrostatic contribution than van der Waals' contribution to the overall energetics of the adsorbent-adsorbate interactions in these materials.[41]

Similarly, replacing bipyridine for pyrazine leads to a much smaller pore in **SIFSIX-3-Zn** relative to its **SIFSIX-1-Zn** counterpart, of 3.84 Å.[22, 40] While **SIFSIX-3-Zn** presents a strong CO_2 binding energy (45 kJ mol^{-1}),[22, 41, 62]it is not as strong as the analogous Cu^{2+} material, **SIFSIX-3-Cu**, which exhibits a slightly smaller pore size but a considerably greater CO_2 interaction energy.[40] This again emphasises the importance of pore size in adsorbent-adsorbate interactions. Also in similarity to **SIFSIX-3-Cu**, **SIFSIX-3-Zn** displays one type of CO_2 sorption[41, 62] where the CO_2 molecule binds in the center of the pore and shows a sharp increase in

Q_{st} at low loading. Due to their small pore size and high CO_2 selectivity, both of these materials offer potential as molecular sieves even at very low partial pressures.

SIFSIX-3-Zn presents a very high C_2H_2 interaction energy (50.3 kJ mol^{-1}). T-shaped co-adsorption was indicated through computation between the C_2H_2 molecules at full loading.[30] The primary site was determined to be between the pyrazine molecules of the unit cell as a result of the dominant electrostatic contribution to the overall energetics, and the secondary site involves weaker $C_2H_2\cdots C_2H_2$ interactions. This was determined from later computational studies concerning another **SIFSIX-3-M'** material, **SIFSIX-3-Ni**.[30] Comprising of a Ni^{2+} metal moiety and a pyrazine linker, **SIFSIX-3-Ni** presents a tight 3.8 Å pore size, a strong CO_2 interaction energy of 50.9 kJ mol^{-1}[36, 41, 61] at low loading and an interaction energy of 36.7 kJ mol^{-1} for C_2H_2 interactions,[30] leading to benchmark CO_2/C_2H_2 performance at low loading (< 0.3 bar).[30, 40] Similar to other **SIFSIX** materials of a pore size < 4 Å, a single CO_2 molecule binds in the centre of each unit cell with the interaction energy predominantly governed by electrostatics. On the contrary, at full loading of C_2H_2, two molecules are present for every binding site, determined to be in a slipped parallel configuration by DFT calculations (delta E = 41.4 kJ mol^{-1}).[30] This same co-adsorption effect is seen in analogous materials with narrow channels. Favourable $CH\cdots F$ interactions are present on one side of every C_2H_2 molecule while the other side undergoes $C_2H_2\cdots C_2H_2$ interactions, indicating that both electrostatics and van der Waals' interactions contribute significantly to the overall energetics.[30] Therefore, at

higher loading, C_2H_2 exhibits favourable binding interactions over CO_2. **SIFSIX-3-Co**, an analogous material to **SIFSIX-3-Ni**, also exhibits highly favourable CO_2 binding energies of 47 kJ mol^{-1} and offers potential in flue gas separation (CO_2/N_2) where **SIFSIX-3-M'** materials show benchmark performance.[61] Although the structural variations between **SIFSIX-3-M'** materials are subtle, it is evident that even the smallest changes in pore size and pore chemistry can lead to significant improvements in CO_2 selectivity by HUMs.[41]

2.1.3 Substituting Si^{2+} for Ti^{2+}: TIFSIX Materials

Recently, variants of the **SIFSIX** family, in which the SiF_6^{2-} anionic linker is substituted for TiF_6^{2-}, have been explored for their potential in gas sorption and separations, named as **TIFSIX** materials.[29, 63, 64] **TIFSIX-2-Cu-i**, an interpenetrated material with a Cu^{2+} node and bipyacetelene linker, presents benchmark C_2H_2/CO_2 performance at low loading in spite of being very similar to **SIFSIX-3-Ni** which separates CO_2/C_2H_2 at low loading.[30] CO_2 loads following a T-shape co-adsorption trend in **TIFSIX-2-Cu-i**, maintaining a Q_{st} of 35.8 kJ mol^{-1} from low to high loading. The larger pore size of 5.15 Å relative to **SIFSIX-3-Ni** (3.8 Å) leads to a primary C_2H_2 binding site in **TIFSIX-2-Cu-i** which effectively serves as a molecular trap for the first four C_2H_2 molecules per unit cell. Each C_2H_2 of this four maintains an independent Q_{st} of 46.3 kJ mol^{-1}, with weak van der Waals' interactions between the guest molecules.[30] However, loading beyond this initial four leads to a

decrease in Q_{st} to 34.2 kJ mol^{-1} to increase loading capacity within the material. Relative to its SiF_6^{2-} counterpart, **TIFSIX-2-Cu-i** exhibits a larger unit cell volume than does **SIFSIX-2-Cu-i** but also a stronger CO_2 binding energy, leading to the suggestion that substitution of the SiF_6^{2-} moiety for TiF_6^{2-} leads to overall better CO_2 selectivity. As Ti^{2+} exhibits stronger electrostatics than Si^{2+}, Ti···F is a longer bond than is Si···F and the equatorial fluorine atoms in the **TIFSIX** variants carry a more negative partial charge. As it has been determined that the electrostatic contribution is greatest to the overall interaction energy between adsorbent and adsorbate, this increase of negative charge within the pore would lead to stronger C···F interactions.[41]

Recognising the effect of pillar substitution, **TIFSIX-3-Ni** was recently synthesised and its gas sorption performance was subsequently compared with existing materials.[29] Although analogous to **SIFSIX-3-Ni** and **NbOFFIVE-1-Ni**, **TIFSIX-3-Ni** exhibits superior performance in terms of its CO_2 Q_{st} (55 kJ mol^{-1}) experimentally at low loading. This is largely attributed to the substitution of **SIFSIX** with **TIFSIX**, shortening *a* and *b* axes, and lengthening the Ti···F bond, leading to more electronegative F atoms and a stronger CO_2 interaction energy. Indeed, PXRD studies indicate that it is the Jahn-Teller effect on the Cu^{2+} atom in **SIFSIX-3-Cu** which likens its PXRD pattern more to **TIFSIX-3-Ni** and **NbOFFIVE-1-Ni** than to other **SIFSIX-3-M'** materials as the fluorine atoms are consequentially more negatively charged.[29, 41] With regard to CO_2 sorption *via* DAC, **TIFSIX-3-Ni**

performs favourably when compared to its **SIFSIX** equivalent, exhibiting benchmark performance in terms of CO_2 selectivity.[29]

2.2 Molecular Simulation of MOMs

While experimental techniques such as crystal engineering and gas sorption analysis by DSC and TGA are useful in distinguishing structural properties and real experimental trends alike, experimental limitations often impede the study of materials at the most fundamental level. Properties such as charge distribution, binding site energetics, and the subtle structural changes which may significantly affect adsorbent-adsorbate interactions are cumbersome if not impossible to analyse in detail by experimental techniques. For this reason, molecular modelling and simulation has been regularly employed to study the properties and behaviour of both real and hypothetical materials where experiment is often disadvantaged in terms of either expense or practical impossibilities. To study metal-organic materials, approaches have included the development of both general and customized empirically derived force-fields to model materials and systems to varying degrees of accuracy, and the implementation of both quantum mechanical and molecular mechanical techniques such as DFT, GCMC and MD, for example.[65, 66]

The use of generic force-fields presents limitations in terms of transferability and accuracy when considering approaches such as large-scale screening.[67] On the

contrary, while many studies implement the use of first-principles based, customised force-fields to accurately model materials and interactions, this method can prove costly in terms of both a monetary and time-consuming investment. In this study, A combined use of DFT and GCMC methods have been employed to best investigate the effects of pyrazine ring configuration on CO_2 sorption in **TIFSIX-3-Ni**, tackling limitations of expense while best conserving accuracy of the interactions investigated in this study. As a result, herein this review focuses primarily on the use of DFT and of GCMC in analysing MOMs, with specific emphasis on the effective use of this approach in analysing HUMs.[68]

2.2.1 Density Functional Theory (DFT)

Throughout the development of hybrid ultramicroporous materials, it has become evident that certain features are key to their favourable interactions with small polarisable gas molecules: a tight pore of ultramicroporous quality and an anionic linker with electronegative F-atoms as the features most differentiating them from other classes of MOMs in terms of both structure and performance.[25, 40, 69] To aid in elucidating such conclusions, computational methods have been heavily employed in determining properties such as binding site positions, possible loading mechanisms and contributions to the energetics of adsorbent-adsorbate interactions.[70] This has been primarily achieved through two methods of molecular simulation, namely

Density Functional Theory (DFT)[13] and Grand Canonical Monte Carlo (GCMC) methods.

DFT is useful for analysing large, periodic systems, particularly those which contain heavy elements, as the computational cost is much lower than methods based on solving for the wave function. Wave function methods typically focus on obtaining orbitals for a single-reference wave function (e.g. Hartree-Fock method (HF)[71]) or multi-reference[72] wave function (e.g. MCSCF and CASSCF) and later adding terms for the dynamical correlation between electrons by post-HF methods to more realistically approximate the system, also scaling much more slowly with the size of the system than DFT. DFT offers a means by which the many-body problem can be systematically mapped onto a system through the use of spatially dependent electron density functionals. Based on the Kohn Sham (KS) theorem,[73] DFT is, in principle, exact for ground state properties as there is a one-to-one correspondence between the electron density and the external potential in which the electrons move. For these reasons, DFT is frequently employed in the computational study of MOFs and MOMs to shed light on the intricacies of a system, such as binding site structure, properties, charge, and interaction energies.[13, 60, 74]

2.2.1.1 Density Functionals

However, as the universal density functional is not known, approximations are made to DFT in the use of density functionals which correct for electron correlation and exchange. Pure or local functionals including local density approximation (LDA), generalised gradient approximation (GGA), nonseparable gradient approximation (NGA) and meta-GGA share the advantage of being significantly cheaper than WFT, but present limitations in the more intricate studies of MOFs. For instance, while LDA is suitable for solid state systems with little variation, it often both overestimates bonding energies and underestimates bond length.[71] Understandably, this is an unsuitable density functional approximation when considering tight binding sites with subtle differences in interaction energies and slight structural variations such as those presented in HUMs.

In attempting to separate electron exchange and correlation, GGA generally gives a better description than does LDA of a system in regions where local variations in the electron density are significant, offering a substantial improvement for calculated ionisation and atomisation energies.[71] Being a local functional, GGA offers computational scalability and accuracy while being significantly cheaper and GGA functionals such as PBE[75] and BLYP[76, 77] have been heavily employed in computational methods concerning extended systems such as MOFs. TPSS[78] and M1 1-L[79] which are meta gradient approximation functionals have also been used in the studies of MOFs for their augmentation of GGA with respect to certain terms.

Although local density functionals have been successfully employed in the computational analysis of MOMs, they share the disadvantage of the exchange and correlation density at a given point depending only on local properties. As a result, hybrid functionals, also denoted as nonlocal functionals, have been derived to account for non-local electron exchange and better account for the energetics of interactions which depend on long range interactions. These functionals are generally derived through a combination of a local functional, e.g. BLYP, and an additional portion of HF exchange which substitutes the exchange term in local approximations. As HF is a nonlocal functional of occupied orbitals, inclusion of a HF based portion offers improved predictions of both reaction energies and of reaction barriers. Hybrid functionals which include this nonlocal exchange include B3LYP[77, 80] and PBE0[81] have been very popular in the field of MOMs, offering significantly better approximations of both energies and barriers where nonlocal exchange becomes important.

All early generation density functionals fail to correctly describe median to long-range correlation effects in system interactions. Damped dispersion, which is a consequence of electron correlation in this range, has a significant impact on the energetics of systems such as MOMs, particularly on the adsorbent-adsorbate interactions in materials with tight binding sites and cannot reasonably be ignored.[74] DFT methods which attempt to correct for this negligence in local functionals add a nonlocal term to the correlation functional and are therefore hybrid density with a

damped dispersion factor, termed as DFT-D.[82] The DFT-D functional offers corrections at van der Waals' distances and include the widely used Grimme terms. However, as the parameters depend on the functional to which they are appended, different errors arise in medium range electron correlation terms depending on different functionals. Evolutions of this functional include the D2[83] and the commonly used D3[84] method, which is not purely pairwise additive and correlates parameters to coordination numbers rather to independent functionals. Overall it remains challenging to accurately model dispersion interactions as a function of charge for metal ions.[74]

With regard to performing electronic structure calculations in MOMs, this is currently achieved through three methods - treating the unit cell with periodic boundary conditions (PBC) to mimic the behaviour of an infinite solid, extending the unit cell into a non-periodic supermolecular cluster to mimic a portion of the material buried in the bulk, and the performance of a mixture of quantum mechanics and molecular mechanics (QM/MM).[74, 85] Supermolecular clusters reduce computational costs when compared to PBC methods, modelling an important subsection of a crystal rather than attempting to mimic an infinite bulk. Many levels of electronic structure theory are available for these systems which are simply too expensive and impractical to be employed in PBC. However, the molecular cluster approach is vulnerable to unphysical edge effects, spatial anisotropy, and the neglect of sometimes significant dispersion interactions. A system under PBC which mimics

an infinite solid does not typically give rise to these inaccuracies and so this is a frequently used approach in the analysis of MOMs, particularly from a gas sorption perspective.[74]

2.2.1.2 Basis Sets and Pseudopotentials

For the performance of periodic DFT methods, basis sets and pseudopotentials are an important in determining both the descriptive accuracy and computational time of the simulation. Plane wave (PW)[86, 87] basis sets are commonly employed, e.g. VASP software, whereby the entire system is represented as a series of plane waves, ensuring completeness and orthonormality in the description of the system. The quality of PW basis sets is uniform at every point in space. Consequently, a large number of basis functions are required to accurately describe which are extended and sparsely packed, as are MOFs.[74] On the other hand, Gaussian basis functions[88] use a combination of GTO orbitals and numerical basis to describe atoms/pseudoatoms in each system. While this is a slower approach than PW, it permits the use of many analysis tools used in periodic calculations and is well suited for parallelisation when orbitals are defined on real-space grids. The Gaussian and Plane-Waves (GPW) method has been implemented in open source code such as CP2K. This method consists of both atom-centered Gaussian orbitals which are used to represent the wave function and of plane waves or regular grids which represent the electron density. The compact representation of the wave function is less computationally expensive and

more efficient when compared to PW representations as only relatively few basis functions are needed per atom. This hybrid algorithm allows for linear scaling methods to optimise the density matrix and compute the Hartree energy in conjunction with Fast Fourier Transforms and screening techniques.

Defining the atoms of a system by pseudopotentials in the periodic DFT approach simplifies the description of the atoms, thus saving on computational time. The pseudopotential approach is grounded in the fact that the valence electrons define most physical and chemical properties of a system. Each pseudoatom consists of a subset of valence electrons involved in self-consistent field (SCF) calculations, i.e. the mean-field determined self-consistently from lowest energy spin-orbitals.[89] The remaining core electrons are replaced with pseudopotentials that mimic their influence on the overall electronic structure. By simplifying the atomic description in this way, both cutoff energies and the required size of the basis set are significantly reduced. Goedecker–Teter–Hutter (GTH) pseudopotentials are designed to be used with plane waves basis sets.[90] As the nonlocal part can be efficiently applied to a wave function in real space, the computation time is faster. Subsequently, GTH potentials are commonly employed in the molecular simulation of MOMs. By the QM/MM approach, an active subsystem of the material is treated by quantum mechanics while the rest of the system is treated by molecular mechanics, allowing the study of larger models. This method is also typically employed with the use of basis sets and pseudopotentials and is a widely used feature of code such as CP2K.

2.3 Charge Fitting

An important part of electronic structure calculations is the assignment of point partial charges to each atom in the system. For MOMs and especially those with tight binding sites such as HUMs, these charges can offer important information as to the distribution of electrons within the material and therefore contributing factors to the overall interaction energetics. Two of the most practiced ways in which partial charges are assigned are by fragmentation[91] and by the REPEAT method. In the fragmentation approach, the material is divided into different fragments in which an atom of interest is buried in a suitable fragment to most accurately capture its chemical environment. The electrostatic potential (ESP) surface is calculated for each fragment and the partial charges subsequently fitted onto atomic positions by methods such as the CHELPG method. Partial charges are then averaged for each chemically distinct atom and adjusted to ensure the neutrality of the system. In theory, this method of charge fitting can be applied to systems of any size as fragments can be chosen to ensure a simulation is computationally tractable. This is a limitation of periodic charge fitting as the computational tractability is dependent on the size of the unit cell. As a result, fragmentation has been widely employed in the molecular simulation of MOMs such as HUMs.

In the REPEAT method, partial charges are fitted to the variance of the electrostatic potential (ESP) as the potential is ill-defined. Fragmentation is not necessary to assign point partial charges to each chemically distinct atom type by this

method. This not only simplifies the process of charge fitting, but as the chemical environment of each atom is described in a way which maintains the structural integrity of the unit cell across an infinite bulk, the risk of compromising the accuracy of each allocated charge is lower with REPEAT than with fragmentation. Restraining the ESP through methods such as RESP, allows chemically distinct atoms to be restrained to a common point partial charge. This better facilitates the accurate point partial charge allocation to heavy atoms in the bulk, which in the case of MOMs, are often metal ions. These metal ions can potentially play a very important role in the adsorbent-adsorbate interactions of materials such as HUMs. For example, the substitution of the SiF_6^{2-} moiety for TiF_6^{2-} in **MFSIX** materials has a dramatic effect on the CO_2 selectivity of the material. For this reason and for the ability to describe a material under PBC, REPEAT and RESP are becoming increasingly popular within the community modelling MOMs. With constant improvement in computational tractability, fitting charges to the electrostatic potential by methods such as REPEAT and RESP is becoming increasingly easier to achieve and the need for fragmentation declines.

2.4 Grand Canonical Monte Carlo (GCMC)

While DFT is useful for studying the energetics of specific interactions and subtle structural properties of systems such as metal-organic materials, often other methods such as GCMC and MD are employed to studying ensemble averages and

dynamical effects after an initial geometry optimisation. In a Grand Canonical Monte Carlo simulation, the chemical potential, volume and temperature of the system are held constant for the duration of the simulation. For calculations involving MOMs, the material is usually held rigid while other particles, e.g. gas molecules, are subjected to random sampling. The rigid structure is typically an optimised structure as output by DFT calculations, complete with point partial charges. Parameters which represent the potential energy surface are chosen from a number of force-fields (FFs), from which the forces can then be analytically calculated. Choosing which parameters are most relevant to the system in question is integral to the accurate computational description of trends such as gas sorption and isosteric heat of adsorption (Q_{st}). For these reasons, care must be taken in choosing from which force field to take parameters. Traditional or generic force fields such as the Universal Force Field (UFF) and DREIDING[92] are typically used to describe most atoms in MOM simulations, and are parameterised to results of electronic structure calculations by first principles or empirically fitted to data which has been obtained experimentally. In the simulation of the **SIFSIX** type materials, customised FFs are often used to describe the system. In this case, most atoms are described using UFF Lennard-Jones van der Waals' parameters, and atoms in a more aromatic environment such as carbons and hydrogens of pyrazine rings are typically treated by OPLS-AA to better describe their chemical environment. Depending on the choice of parameters, simulation results can vary greatly. At the ultramicroporous level, induced polarisation has the potential to play a large part in the energies of interactions. When included explicitly in classical force-fields,

polarisability is most commonly accounted for with a Thole-Applequist model, wherein the included atomic dipoles are solved in a many-body and self-consistent manner. Concerning the sorption of CO_2 in HUMs, it has become apparent that correctly accounting for the induced polarisation of the CO_2 molecule is crucial to accurately modelling the energetics of the adsorbate-adsorbent interactions. In the case of the **MFSIX** family of materials, this is accounted for by employing a rigid, five-site polarisable potential for CO_2 where parameters are fit to highly accurate *ab initio* data.

Chapter 3: Methods

In this study, two methods of molecular modelling are employed to study the effect of subtle variations in the pyrazine rings on CO_2 sorption in **TIFSIX-3-Ni**, namely Density Functional Theory (DFT) and Grand Canonical Monte Carlo (GCMC).[93] DFT was employed to computationally model the microscopic physical properties of the system whereas Grand Canonical Monte Carlo (GCMC) methods were employed to investigate the effect of different pyrazine ring configurations upon low-pressure CO_2 uptake and Q_{st}.

Three distinct, rigid systems were chosen for this study, defined herein as $Sys_{(8,0)}$, $Sys_{(6,2)}$ and $Sys_{(4,4)}$, comprising of a total of five chemically distinct binding sites: 8-in, 6-in, 4-in, 2-in, and 0-in (Figure 4). All systems were created by eliminating pyrazine ring disorder from the PXRD determined crystal structure, using Materials Studio. These 2 x 2 x 2 systems were labelled in accordance with the ratio of pyrazine edges and faces interacting with the guest molecule; they represent variations of the smallest obtainable unit cell after eliminating disorder. The binding sites studied differ in pyrazine ring orientation and therefore slightly different pore size and chemistry; they are equivalent along diagonal vertices in each system. The names assigned to the binding sites indicate the number of pyrazine rings pointing toward the adsorbate molecule at the center of each site. $Sys_{(8,0)}$ comprises of two distinct binding sites, 8-in and 0-in, and represents the system of greatest contrast in terms of binding sites of both different pore size and pore chemistry. $Sys_{(4,4)}$ presents two 4-in sites which are

chemically equivalent, and represents a more homogenous and isotropic environment. $Sys_{(6,2)}$ comprises of a 6-in site and 2-in site, and is representative of an asymmetrical intermediate between the previously defined structures, allowing for the analysis of potential directional loading bias.

All systems in this study were created from experimentally obtained unit cell parameters by PXRD, in which the pyrazine rings were observed to be disordered over two sites. The equatorial fluorine atoms of the SiF_6^{2-} anion were fixed at an angle of 45° with respect to the *a*-axis which is in agreement with PXRD data and was found to be the optimal positioning in a similar HUM, **SIFSIX-3-Ni**, in a previous computational study.[40] In the study of **SIFSIX-3-Ni**, simulations supported the hypothesis that a smaller pore size in HUMs is proportional to the strength of the binding interaction energy with small polarisable molecules such as CO_2.[40] Similarly, another computational study conducted on **SIFSIX-3-Ni** indicated that the rotational configurations of the pyrazine rings may affect Xe interactions.[42] These hypotheses formed the basis for this study which served to investigate if a similar effect of pyrazine ring configuration on CO_2 interactions was relevant for **TIFSIX-3-Ni**.

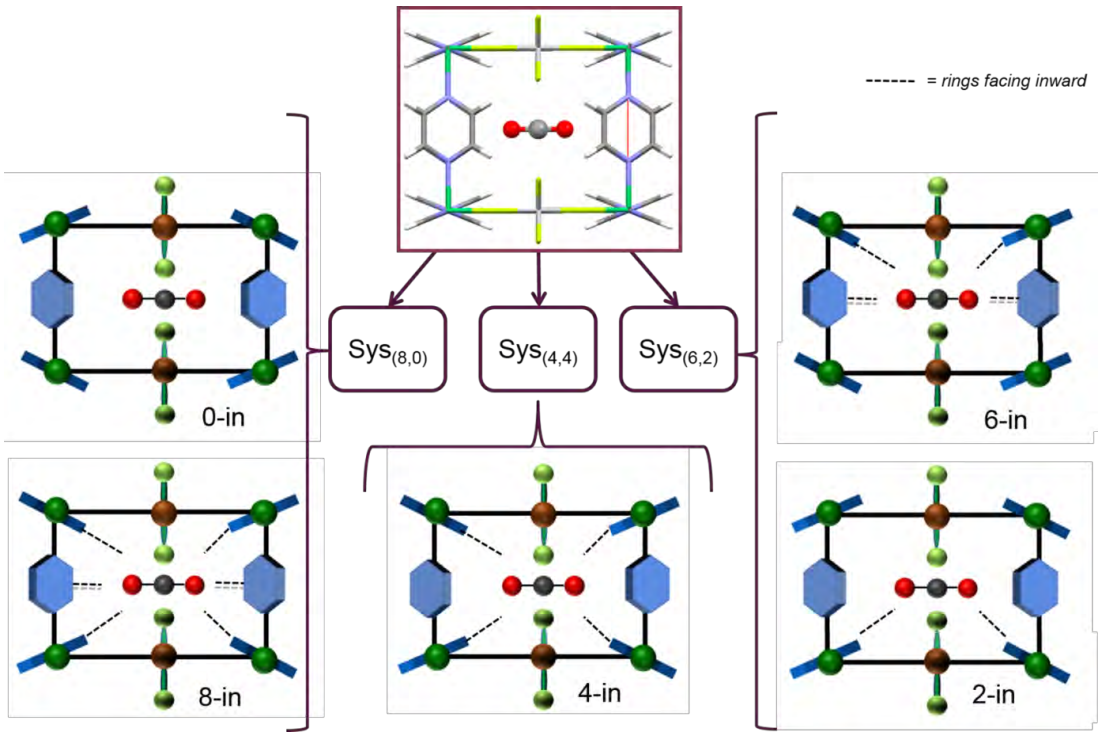

Figure 4: Schematic of systems studied and corresponding pyrazine ring orientations.

These computationally constructed systems were geometry optimised by DFT using the Quickstep Gaussian and Plane-Waves method (GPW) of CP2K open source code.[94-96] Goedecker–Teter–Hutter (GTH) pseudopotentials and the gradient-correct BLYP functional were employed in DFT simulations.[76, 77, 90] A plane-wave energy cut off of 400 Ry was chosen to best preserve both efficiency and accuracy of the model. All atoms were represented by a double zeta plus polarisation basis set (DZVP-MOLOPT).[97] Using the REPEAT method, partial atomic charges were fitted to the variance of the potential.[98]

The electron density was solved self-consistently with an SCF convergence factor of 1E-6. A BLYP exchange-correlation was employed along with the nonlocal rVV10 functional and C9 corrections to capture long-range dispersion interactions.[77] A multiplicity of 17 was applied to the system under an unrestricted Kohn-Sham (UKS) model to capture the spin state of the octahedral Nickel. Cell lengths were defined as $a = b = 13.99570$ Å and $c = 15.58720$ Å , with angles $\alpha = \beta = \gamma = 90°$, assuming tetragonal symmetry. Periodic boundary conditions were employed to assume infinite replication of the unit cell in XYZ directions. Calculations were continued until convergence was achieved. For geometry optimisations, the maximum number of inner SCF iterations of 40 was used with a maximum number of outer SCF iterations of 20 to a convergence factor of 5E-6, to allow rotation and relaxation of the atoms and in particular, of the pyrazine rings. A conjugate gradient optimiser was employed and cell parameters were fixed by maintaining initial symmetry as defined by the input file.

The sorption of CO_2 in **TIFSIX-3-Ni** for each system was studied by GCMC simulations using MPMC software.[99] By this method, the chemical potential, volume and temperature of the adsorbent/sorbate system were constrained to be constant while other thermodynamic variables were free to fluctuate.[100] Input pqr files were generated using cartesian coordinates from pdb files as generated by MS. Partial atomic charges for each chemically distinct atom were assigned according to the results of the REPEAT method during the DFT calculations.[98] Two series of

simulations were run - one in which all atoms of the system were parameterised by UFF van der Waals' parameters[66] and one in which all CH adsorbent moieties were modelled by OPLS-AA van der Waals' parameters[65] while the rest of the atoms were assigned UFF van der Waals' parameters. The induced CO_2 dipole was accounted for by employing a rigid, five-site polarisable potential for CO_2 where parameters are fit to highly accurate *ab initio* data.[101]

Throughout the course of the simulation, sorbate molecules were randomly inserted, deleted, translated or rotated with acceptance or rejection based on a random number generator weighted by the energetic favourability of the move. The adsorbent atoms remained fixed in their positions as were initially defined in the input pqr file. Periodic boundary conditions applied as they were in DFT optimisation calculations, to approximate the macroscopic environment of **TIFSIX-3-Ni**; half of the shortest system cell dimension length defined the spherical cut-off point for the boundary. The average particle number was calculated by the following expression:[102, 103]

$$\langle N \rangle = \frac{1}{\Xi} \sum_{N=0}^{\infty} e^{\beta \mu N} \left\{ \prod_{i=1}^{3N} \int_{-\infty}^{\infty} dx_i \right\} N e^{-\beta U(x_1, \ldots, x_{3N})}$$

where Ξ represents the grand canonical partition function, β represents the quantity $1/kT$ where k is the Boltzmann constant, and the total potential energy is defined by U.

The Peng-Robinson equation of state was used to define the chemical potential for CO_2, μ.[104] U was calculated as the sum of the repulsion/dispersion energy as calculated by the Lennard-Jones 12-6 potential,[105] the stationary electrostatic energy as calculated by use of Ewald summation,[106, 107] and the many-body polarisation energy contribution to the total potential energy represented by U_{rd}, $U_{es}$and U_{pol} respectively:

$$U = U_{rd} + U_{es} + U_{pol}$$

U_{pol} was explicitly calculated using a Thole-Applequist type model.[108-112] The interactions between unlike species were generated by the Lorentz-Bertholet mixing rules for calculation of the repulsion/dispersion energy.[113] Upon the calculation of the number of particles, $\langle N \rangle$, this was converted to a value equivalent to the experimental quantity for CO_2 uptake for each state point considered.

The experimental Q_{st} of CO_2 for **TIFSIX-3-Ni** was previously calculated from low pressure CO_2 adsorption isotherms collected at 273, 283 and 293 K using the Clausius-Clapeyron equation and virial-type equations (below) to fit ten adsorption points between 0 and 0.3mbar.

$$\ln P = \ln n + (\frac{1}{T^2}) \sum_{i=0}^{j} a_i n^i + \sum_{i=0}^{k} b_i n^i$$

$$-Q_{st} = -R \sum_{i=0}^{j} a_i n^i$$

Values for the simulated isosteric heat of adsorption, Q_{st}, were calculated using an expression based on fluctuations in particle number, N, and total potential energy, Uat constant temperature 293K:[114]

$$Q_{st} = -\frac{\langle NU\rangle - \langle N\rangle\langle U\rangle}{\langle N^2\rangle - \langle N\rangle^2} + kT$$

Simulations consisted of 1E-6 Monte Carlo steps for all state points considered in **TIFSIX-3-Ni**, to guarantee equilibration and ensure reasonable ensemble averages for $\langle N\rangle$ and Q_{st}.[99]

Explicit polarisation was included in all simulations via a Thole-Applequist induced dipole model.[109, 111, 112] Dipole polarisabilities for all C, H, N and F atoms were taken from the set of van Duijnen et al. while the polarisabilities for Ti and Ni were determined in previous studies.[108] A polarisable, five-site CO_2 model, CO_2-PHAST*, was used throughout the simulations in this work.[101]

Chapter 4: Results and Discussion

4.1: DFT Geometry Optimisations and Charge Fitting

DFT geometry optimisations revealed that the pyrazine rings are free to rotate around approximately ± 2° from 14.58° as determined by PXRD. For GCMC calculations, the pyrazine ring angle was therefore constrained to be 14.58° for the purpose of better comparing the effect of pyrazine ring orientation between the analysed systems with fewer variables to influence the energetics and structures of these binding sites. The CH bond lengthened to 1.038 Å upon relaxation by DFT. This bond length was imposed in the rigid systems used for GCMC calculations. Partial atomic charges which were calculated for each adsorbent atom by the REPEAT method,[98] with chemically distinct atoms constrained to have the same partial charges, are reported in the table below. In the cases of both $Sys_{(8,0)}$ and $Sys_{(4,4)}$ which both present two, symmetrical binding sites, each element shared the same partial atomic charge with the exception of fluorine atoms, which were distinguished chemically by their equatorial and axial positions about the Ti atom. For $Sys_{(6,2)}$, two asymmetrical binding sites are presented (6-in and 2-in) and so the distribution of partial charge was allocated to four different atom types for each chemical species with the exception of fluorine atoms which were allocated six different sets of partial atomic charges based due to their position about Ti^{2+} and the binding sites to which they belong.

Table 1: Partial charges in elementary electric charge (**e**) for the atoms within the unit cell of **TIFSIX-3-Ni** as determined through periodic charge fitting calculations on the system using CP2K. Pyrazine ring angle fixed at 14.58°.

System	**Sys$_{(6,2)}$**	**Sys$_{(4,4)}$**	**Sys$_{(8,0)}$**
Atom Type	***q*** **(e)**	***q*** **(e)**	***q*** **(e)**
C1	0.00342	-0.02200	-0.02600
C2	-0.05345	x	X
C3	-0.01946	x	X
C4	-0.00742	x	X
H1	0.14066	0.15420	0.14500
H2	0.15818	x	X
H3	0.14258	x	X
H4	0.14726	x	X
Ni1	0.42120	0.41800	-0.37900
Ni2	0.40860	x	X
Ti1	1.71336	1.67700	1.70200
Ti2	1.68400	x	X
F1	-0.46422	-0.46030	-0.45590
F2	-0.54986	-0.53700	-0.53110
F3	-0.52765	x	X
F4	-0.46422	x	X
F5	-0.53930	x	X
F6	-0.45465	x	X
N1	-0.04182	-0.02100	0.10000
N2	0.02364	x	X
N3	-0.01084	x	X
N4	-0.04858	x	X
COE	0.385670	0.385670	0.385670

4.2: CO_2 Adsorption Isotherms

Grand Canonical Monte Carlo simulations were conducted to produce both simulated CO_2 adsorption isotherms and Q_{st} plots for comparison with those which were experimentally obtained. Isotherms were plotted in terms of percentage weight (wt%) of CO_2 in **TIFSIX-3-Ni** as a function of pressure of the external CO_2 reservoir, scaled in accordance with experiment. The results of these simulations reveal little difference with respect to CO_2 loading in each system, but a significant difference was observed between the trends of data which was modelled with entirely UFF van der Waals' parameterisation and that in which OPLS-AA van der Waals' parameters we applied to aromatic CH moieties. Upon comparison with the experimentally determined trend for CO_2 loading, it was observed that the experimental trend approximated van der Waals' properties intermediate between the two series of data analysed by simulation.

The similarity in CO_2 trend for $Sys_{(8,0)}$, $Sys_{(6,2)}$ and $Sys_{(4,4)}$ regardless of van der Waals' parameterisation was indicative of little effect of the pyrazine ring orientation on the loading capacity of **TIFSIX-3-Ni** for CO_2 under the conditions for simulation. As the adsorbent was constrained to be rigid throughout the course of simulation, it was noted that the 8-in binding site was preferably loaded with CO_2 in $Sys_{(8,0)}$ relative to 0-in sites This trend was also exhibited in $Sys_{(6,2)}$ in which 6-in sites loaded before 2-in sites, indicating that with more pyrazine rings pointing toward the CO_2 at the center of the cell, the binding energy is enhanced. In $Sys_{(4,4)}$, each possible

binding site was chemically equivalent and so this distinction was not observed (Figure 5).

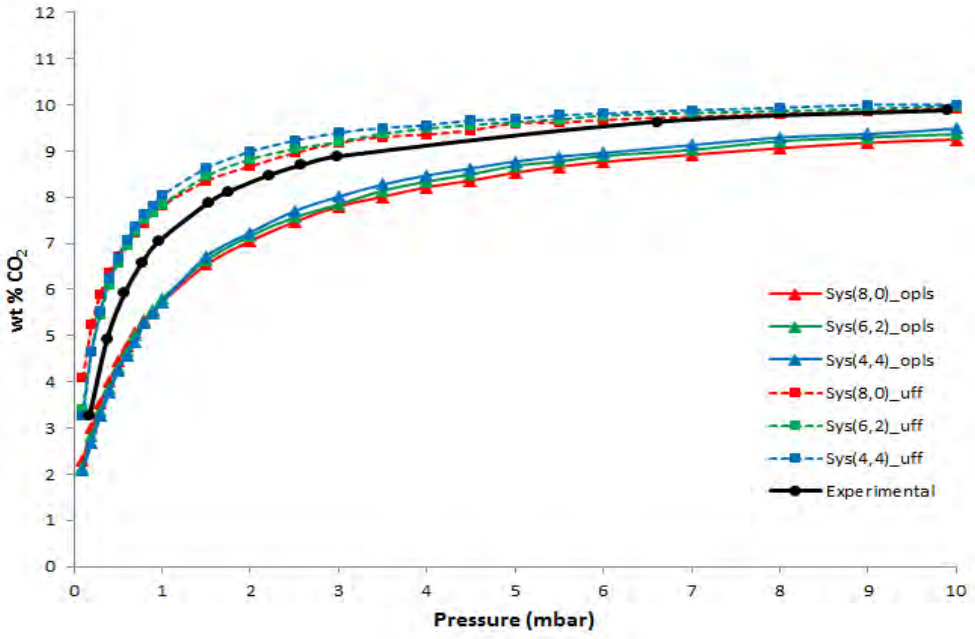

Figure 5: CO_2 loading in rigid 2 x 2 x 2 **TIFSIX-3-Ni** configurations with pyrazine ring angle 14.58°. $Sys_{(8,0)}$ red, $Sys_{(6,2)}$ green, $Sys_{(4,4)}$ blue, experiment (black). Simulations conducted with OPLS-AA Lennard-Jones parameters are represented by triangles (▲) with UFF parameters represented by squares (■).

4.3: CO_2 Isosteric Heat of Adsorption

Experimentally, the CO_2 Q_{st} trend **TIFSIX-3-Ni** was observed to decrease at greater than 50% loading. The Q_{st} trends observed for simulated systems were in agreement with experimental data for both series of van der Waals' parameterisation. $Sys_{(8,0)}$ exhibited the steepest Q_{st} descent followed by $Sys_{(6,2)}$, while in the case of $Sys_{(4,4)}$, the decreasing trend was less pronounced. This is in agreement with results from isotherm simulations which indicated a preference for the loading of sites with more edge-to-guest interactions before loading the remaining sites with a lower CO_2 binding energy. As $Sys_{(8,0)}$ presents the most extreme binding sites and $Sys_{(4,4)}$ exhibits increased homogeneity across the system, the differences in the gradient of the simulated Q_{st} trends is also in agreement with this hypothesis. As the experimental Q_{st} trend for **TIFSIX-3-Ni** decreases after 50% loading, it is suggested that the effect of pyrazine ring orientation on CO_2 binding affinity in **TIFSIX-3-Ni** in simulation studies is relevant to what occurs experimentally. As the coexistence of multiple pyrazine ring configurations cannot be determined *in situ* PXRD, the possibility of this coexistence as demonstrated in this study could explain the position of the experimental Q_{st} curve relative to the simulated Q_{st} curves of $Sys_{(8,0)}$ and $Sys_{(6,2)}$ (Figure 6).

Experimentally, the Q_{st} curve for CO_2 in **TIFSIX-3-Ni** is seen to rise from initial loading to approximately 50%. Unfortunately, it was not possible to capture this effect by the computational approach used in this study. Limitations of the MPMC code dictate that no fewer than one adsorbent molecule can be present in the system at any one time, meaning that in spite of lowering the pressure, it is the system size which ultimately yields the number of data points that can be collected for Q_{st} illustration by GCMC methods. In this study, 2 x 2 x 2 systems were studied as this was determined to be the smallest unit cell after ordering and fixing the positions of the pyrazine rings. As MPMC requires the implementation of periodic boundary conditions, PBC, the next system which could be analysed by this method would be of 4 x 4 x 4 size relative to the xyz parameters of the disordered unit cell. This would significantly increase the computational time and would be unfeasible to study.

While more data points could be collected for the system under this parameterisation, it is estimated that the initial increase in Q_{st} as observed experimentally could be a consequence of initially ordering the pyrazine rings from a state of disorder over two sites to fixing their positions in a manner which would enhance the binding affinity of the first CO_2 molecule. This would require rings in all adjacent cells to consequently order as well, leading to the presence of at least two binding sites across the system, therefore suggesting possible co-adsorption of CO_2 in this material. As systems were held rigid for GCMC calculations, this initial rise in Q_{st} would not be captured by this computational approach regardless of system size. It is

therefore of interest to research the effect of ring rotation on Q_{st} and loading of CO_2 in **TIFSIX-3-Ni** in future studies by other methods such as DFT.

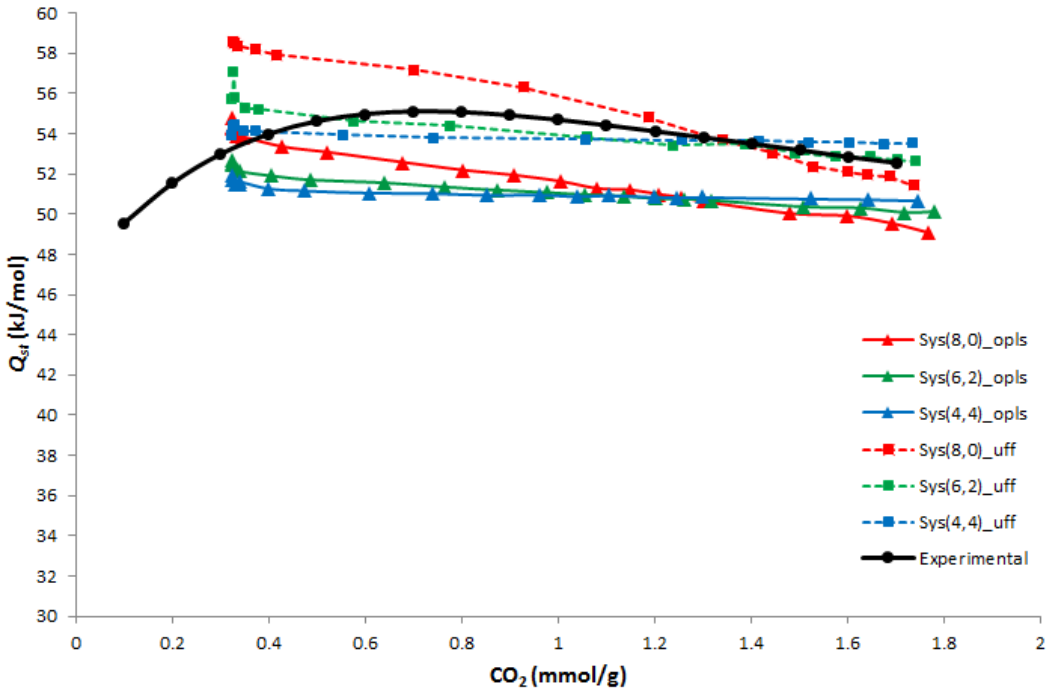

Figure 6: Isosteric heat of adsorption (Q_{st}) for **TIFSIX-3-Ni** systems, simulated at 298K. $Sys_{(8,0)}$ red, $Sys_{(6,2)}$ green, $Sys_{(4,4)}$ blue, experiment (black). Simulations conducted with OPLS-AA Lennard-Jones parameters are represented by triangles (▲) with UFF parameters represented by squares (■). Pyrazine ring angle of 14.58°

4.4 Single Point Energy Calculations

Single point energy calculations were conducted for larger 4 x 4 x 4 systems using MPMC, to ensure a better approximation of the CO_2 binding energy in the static system. These systems comprise of a total of 64 binding sites, and so to determine the binding energy of CO_2 in an individual site type, CO_2 molecules were manually placed in the 32 sites specific to any one binding site type e.g. 8-in. The resulting energy was then divided by 32 to determine the binding energy of CO_2 in each individual site. These calculations reveal that the CO_2 binding energy is proportional to the number of edge-to-guest interactions in line with what was suspected from isotherm and Q_{st} plots. A difference of 4.85 kJ mol^{-1} was indicated between the most and least favourable sites, 8-in and 0-in, with CH moieties parameterised by OPLS-AA Lennard Jones parameters (Table 3). This difference increased to 7.30 kJ mol^{-1} with UFF parameterisation, indicating a significant difference between the binding energies of these sites regardless of which van der Waals' parameters were taken into account. In fully loaded systems, more isotropic conditions were determined to be favourable for CO_2 binding sites as both $Sys_{(4,4)}$ and $Sys_{(6,2)}$ systems were energetically favourable to $Sys_{(8,0)}$. This further suggests the possibility of coexistence of multiple pyrazine ring configurations as **TIFSIX-3-Ni** is loaded (Table 2).

Table 2: Calculated adsorption energies (in kJ mol^{-1}) for a single CO_2 molecule within the unit cell of each fully loaded 2 x 2 x 2 system for **TIFSIX-3-Ni** studied as determined from classical single point energy calculations using MPMC using **(i)** OPLS-AA van der Waals' parameters for C and H atoms and **(ii)** using UFF van der Waals' parameters for all atoms. Pyrazine ring angle of 14.58°

System	(i) ΔE (kJ mol^{-1})	(ii) ΔE (kJ mol^{-1})
$Sys_{(8,0)}$	-51.18	-54.42
$Sys_{(6,2)}$	-52.42	-55.21
$Sys_{(4,4)}$	-52.39	-55.18

Table 3: Calculated adsorption energies (in kJ mol^{-1}) for a single CO_2 molecule within the unit cell of each chemically distinct binding site simulated for **TIFSIX-3-Ni** studied as determined from classical single point energy calculations using MPMC using **(i)** OPLS-AA van der Waals' parameters for C and H atoms and **(ii)** using UFF van der Waals' parameters for all atoms. Pyrazine ring angle of 14.58°

Binding Site	(i) ΔE (kJ mol^{-1})	(ii) ΔE (kJ mol^{-1})
8in	-54.07	-58.54
6in	-54.46	-57.69
4in	-52.60	-55.36
2in	-51.32	-53.67
0in	-49.22	-51.24

4.5 Effect of Pyrazine Ring Tilting

Although the energy cost of rotating and ordering pyrazine rings was not investigated in this study, it was noted that slight variations in the angle of the pyrazine rings could have a significant effect on the binding site due to the tightness of the pore. In light of this, systems with a slightly greater ring tilt angle of approximately 22° (22.104°) were modelled by the methods earlier described. This slight variance in ring tilt angle produced significantly different simulation results. Single point energy calculations revealed a similar trend to that which was observed for systems with a ring tilt angle of 14.58°, indicating that by increasing the number of edge-to-guest interactions the CO_2 binding energy was enhanced. The difference between the binding energies of CO_2 in the most and least preferable sites was observed to be greater for systems with a greater tilt angle (9.3 kJ mol^{-1} for OPLS). When modelled by UFF, 6-in and 4-in sites were determined to present a greater binding energy for CO_2 adsorption. This was attributed to overestimation of the repulsion/dispersion contribution in these systems as a result of greater overlap between pyrazine rings due to a greater ring tilt angle. Consequently, the OPLS series was determined to more accurately reflect experimental data under these conditions. (Tables 4 and 5)

Table 4: Calculated adsorption energies (in kJ mol^{-1}) for a single CO_2 molecule within the unit cell of each fully loaded 2 x 2 x 2 system for **TIFSIX-3-Ni** studied as determined from classical single point energy calculations using MPMC. Pyrazine ring angle of 22.104°

System	ΔE (kJ mol^{-1})
Sys(8,0)	-53.71
Sys(6,2)	-55.12
Sys(4,4)	-56.77

Table 5: Calculated adsorption energies (in kJ mol^{-1}) for a single CO_2 molecule within each binding site studied for **TIFSIX-3-Ni** as determined from classical single point energy calculations using MPMC.Pyrazine ring angle of 22.104°

Binding Site	ΔE (kJ mol^{-1})
8in	-58.92
6in	-58.08
4in	-57.36
2in	-53.37
0in	-49.65

This too was reflected in simulated isotherm plots by GCMC (Figure 7). The greater tilt in the pyrazine ring angle lead to a significant difference in the loading behaviour of CO_2 in **TIFSIX-3-Ni**. Unlike the trend which was seen for systems with a ring angle of 14.58°, trends observed for systems with a greater ring angle differed

with different ring orientations rather than by van der Waals' parameterisation. $Sys_{(8,0)}$ best approximated experimental data while $Sys_{(6,2)}$ and $Sys_{(4,4)}$ overestimated the experimental trend. Similarly, 8-in sites loaded before 0-in sites and 6-in before 2-in, again leading to the suggestion that the edge-to-guest interactions significantly affect the binding energy of CO_2 and become increasingly important with the tightness of the pore.

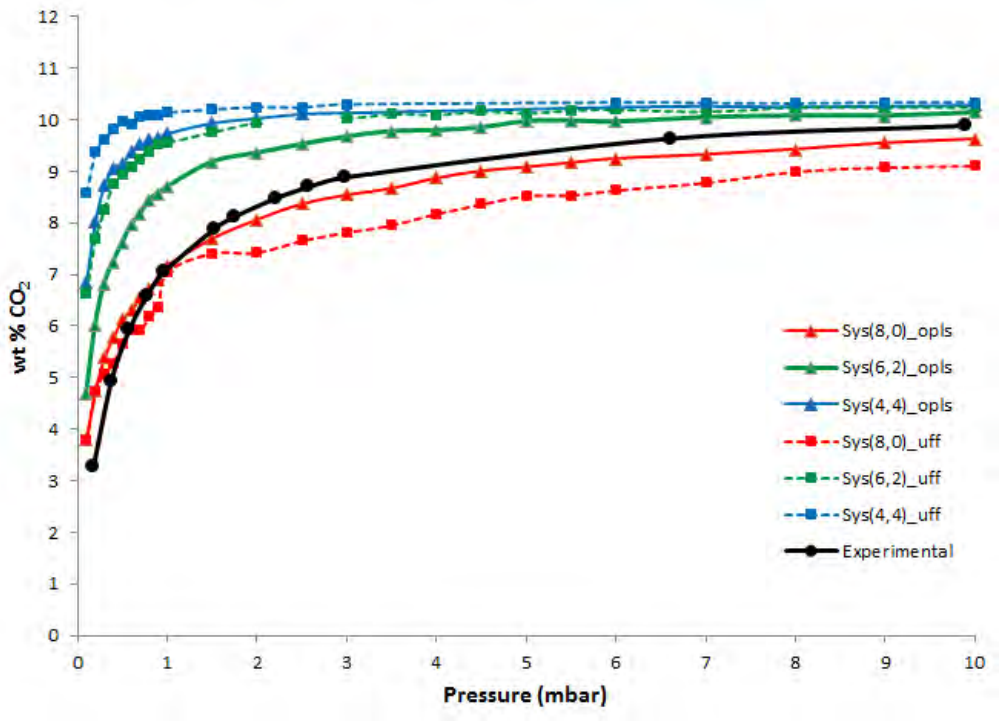

Figure 7: CO_2 loading in rigid 2 x 2 x 2 **TIFSIX-3-Ni** configurations with pyrazine ring angle 22.104°. $Sys_{(8,0)}$ red, $Sys_{(6,2)}$ green, $Sys_{(4,4)}$ blue, experiment (black). Simulations conducted with OPLS-AA Lennard-Jones parameters are represented by triangles (▲) with UFF parameters represented by squares (■).

Q_{st} plots were generated as before for systems with a ring tilt angle of 22.104°. A similar trend to that which was observed for systems with a pyrazine ring angle

equivalent to that which was determined by in situ PXRD was observed for this system, but the effect of pyrazine ring orientation on Q_{st} was exaggerated (Figure 8). A steep descent was observed for the $Sys_{(8,0)}$ trend, while a subtler gradient was observed for $Sys_{(6,2)}$ and $Sys_{(4,4)}$. For each system, Q_{st} trends overestimated the experimental trend at initial loading and in the case of $Sys_{(4,4)}$ throughout the simulation. The decreasing trend which was observed experimentally was also exhibited in systems $Sys_{(8,0)}$ and $Sys_{(6,2)}$, or rather the systems studied which present a favourable binding site.

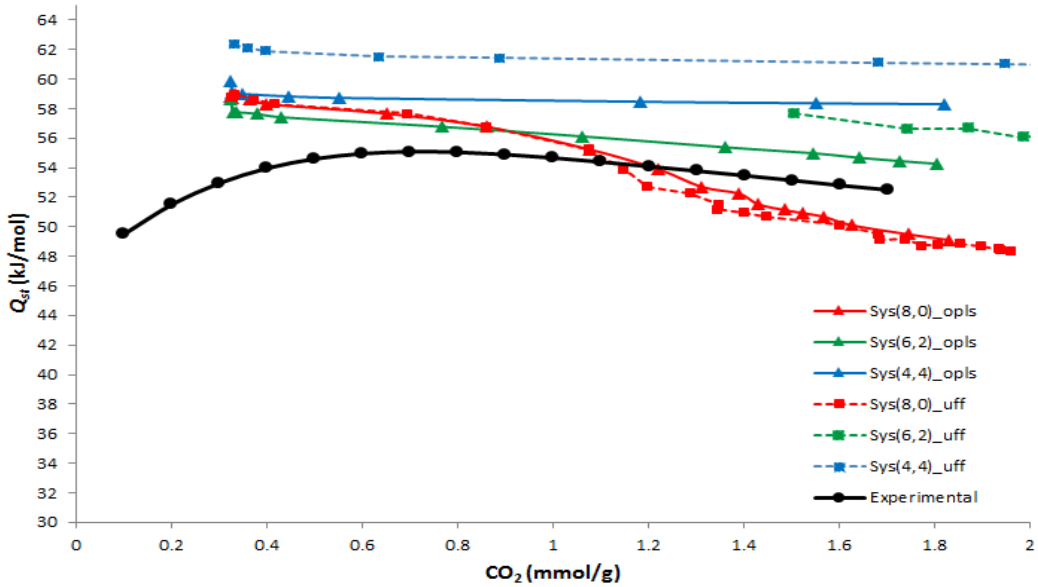

Figure 8: Isosteric heat of adsorption of CO_2 in rigid 2 x 2 x 2 **TIFSIX-3-Ni** configurations with pyrazine ring angle 22.104°. $Sys_{(8,0)}$ red, $Sys_{(6,2)}$ green, $Sys_{(4,4)}$ blue, experiment (black). Simulations conducted with OPLS-AA Lennard-Jones parameters are represented by triangles (▲) with UFF parameters represented by squares (■).

To further question the importance of the pyrazine ring tilt angle, single point energy calculations were carried out for systems with a ring tilt angle of 7.0° and 28.0° respectively. With a pyrazine ring tilt angle of 28.0° extremely repulsive values were returned for the binding energy of CO_2 in each site with the exception of 6-in and 2-in, indicating that at this systems with this extreme angle do not at all approximate experimental data. In light of this, the values obtained for single point energies for this system have not been reported in this study. Systems with a ring tilt angle of 7.0° exhibit a similar trend to those with angles of 14.58° and 22.104°, whereby the binding affinity of the material for CO_2 is proportional to the number of edge-to-guest interactions (Table 6). However, the difference between the binding energies of the most preferable (8in) and least preferable (0in) sites were negligible (2.25 OPLS and 3.11 UFF) (Table 7). These results merit further study of the effect of ring rotation and tilting on the binding affinity of CO_2 in **TIFSIX-3-Ni**, across a range of values less than 14.58° and greater than 22.104°.

Table 6: Calculated adsorption energies (in kJ mol^{-1}) for a single CO_2 molecule within the unit cell of each fully loaded 2 x 2 x 2 system for **TIFSIX-3-Ni** studied as determined from classical single point energy calculations using MPMC using **(i)** OPLS-AA van der Waals' parameters for C and H atoms and **(ii)** using UFF van der Waals' parameters for all atoms. Pyrazine ring angle 7.0°

System	(i) ΔE (kJ mol^{-1})	(ii) ΔE (kJ mol^{-1})
$Sys_{(8,0)}$	-51.09	-53.80
$Sys_{(6,2)}$	-51.69	-54.40
$Sys_{(4,4)}$	-29.25	-31.97

Table 7: Calculated adsorption energies (in kJ mol^{-1}) for a single CO_2 molecule within the unit cell of each chemically distinct binding site simulated for **TIFSIX-3-Ni** studied as determined from classical single point energy calculations using MPMC using **(i)** OPLS-AA van der Waals' parameters for C and H atoms and **(ii)** using UFF van der Waals' parameters for all atoms. Pyrazine ring angle of 7.0°.

Binding Site	(i) ΔE (kJ mol^{-1})	(ii) ΔE (kJ mol^{-1})
8in	-52.6939	-55.8431
6in	-52.8337	-55.7672
2in	-51.5138	-53.67
0in	-50.4483	-52.7342

Chapter 5: Conclusions and Future Work

It is evident from this study that the orientation of the pyrazine rings about the CO_2 binding site in **TIFSIX-3-Ni** significantly affects the binding affinity of CO_2 in the site. It is also indicated that this binding energy is proportional to the number of edge-to-guest interactions present in the site, increasing with the number of pyrazine rings pointing toward the centre of the cell. When compared with experimentally obtained data, molecular simulation indicates that multiple configurations of pyrazine ring orientation about a site may coexist as **TIFSIX-3-Ni** is loaded with CO_2, shedding light on potential loading mechanisms of the material in which experiment is impeded. When vacated, **TIFSIX-3-Ni** exhibits pyrazine ring disorder about two sites as determined by *in situ* PXRD and the rings can more freely rotate in the absence of a CO_2 molecule. Upon the presence of a CO_2 molecule in site, rotating and fixing pyrazine rings to optimise the edge-to-guest interaction energy would lead to an energy cost which could explain the unusual Q_{st} plot observed experimentally. For the systems modelled in this study, all preferable binding sites would be loaded at 50% loading and so the system could in theory relax to a more isotropic or disordered configuration beyond this point to increase the capacity for CO_2 uptake across the system as a whole. Such a mechanism could offer a plausible explanation as to the why the Q_{st} trend observed experimentally increases upon initial loading before later decreasing.

The degree to which the pyrazine rings are tilted about the binding site was also shown to significantly affect the binding energy of CO_2 in the site. This again highlights the importance of pore size in the potential of hybrid ultramicroporous materials for the adsorption of small polarisable materials, as even subtle variations in structural dynamics can significantly impact the interaction energies of potential binding sites. It is interesting to note the importance of van der Waals' parameterisation in modelling these materials. In the case of **TIFSIX-3-Ni**, van der Waals' parameters intermediate to the data series run in this study, denoted by OPLS and UFF, were shown to best approximate experiment when the unit cell was based on *in situ* PXRD results. Upon exaggeration of the pyrazine ring angle for investigative purposes, slight differences in Lennard-Jones parameters are observed to have a significant effect on both qualitative and quantitative results. Consequently, care should be taken when modelling the repulsion/dispersion of such structurally sensitive materials. Future work will aim to further investigate the effect of pyrazine ring tilting and of ring rotation on the binding energy of CO_2 within the site, in an attempt to model the unique increasing Q_{st} trend observed experimentally and to better understand the gas sorption performance of **TIFSIX-3-Ni** and hybrid ultramicroporous materials. This study also highlights the importance of developing synergy between molecular modelling and experiment for the purposes of testing, validating and advancing modelling methods, and ultimately to guide materials design.

References

1. Olivier, J.G., G. Janssens-Maenhout, and J.A. Peters, *Trends in Global CO_2 Emissions: 2012 Report. PBL Netherlands Environmental Assessment Agency and Institute for Environment and Sustainability of the European Commission's Joint Research Centre: The Hague/Bilthoven, 2012*. 2013.
2. Metz, B., et al., *IPCC special report on carbon dioxide capture and storage*. 2005, Intergovernmental Panel on Climate Change, Geneva (Switzerland). Working Group III.
3. Zeman, F.S. and K.S. Lackner, *Capturing carbon dioxide directly from the atmosphere.* World Resource Review, 2004. **16**(2): p. 157-172.
4. Sanz-Pérez, E.S., et al., *Direct capture of CO_2 from ambient air.* Chemical reviews, 2016. **116**(19): p. 11840-11876.
5. Hufton, J., S. Mayorga, and S. Sircar, *Sorption-enhanced reaction process for hydrogen production.* AIChE Journal, 1999. **45**(2): p. 248-256.
6. McDonald, T.M., et al., *Cooperative insertion of CO_2 in diamine-appended metal-organic frameworks.* 2015.
7. Boot-Handford, M.E., et al., *Carbon capture and storage update.* Energy & Environmental Science, 2014. **7**(1): p. 130-189.
8. Li, B., et al., *Emerging multifunctional metal–organic framework materials.* Advanced Materials, 2016.
9. Sumida, K., et al., *Carbon dioxide capture in metal–organic frameworks.* Chem. Rev, 2012. **112**(2): p. 724-781.
10. Perry Iv, J.J., J.A. Perman, and M.J. Zaworotko, *Design and synthesis of metal–organic frameworks using metal–organic polyhedra as supermolecular building blocks.* Chemical Society Reviews, 2009. **38**(5): p. 1400-1417.
11. Rosi, N.L., et al., *Hydrogen storage in microporous metal-organic frameworks.* Science, 2003. **300**(5622): p. 1127-1129.

12. Arstad, B., et al., *Amine functionalised metal organic frameworks (MOFs) as adsorbents for carbon dioxide.* Adsorption, 2008. **14**(6): p. 755-762.
13. Torrisi, A., R.G. Bell, and C. Mellot-Draznieks, *Functionalized MOFs for enhanced CO_2 capture.* Crystal Growth & Design, 2010. **10**(7): p. 2839-2841.
14. Batten, S.R., S.M. Neville, and D.R. Turner, *Coordination polymers: design, analysis and application*. 2009: Royal Society of Chemistry.
15. Kitagawa, S., R. Kitaura, and S.i. Noro, *Functional porous coordination polymers.* Angewandte Chemie International Edition, 2004. **43**(18): p. 2334-2375.
16. Farrusseng, D., *Metal-organic frameworks: applications from catalysis to gas storage*. 2011: John Wiley & Sons.
17. MacGillivray, L.R., *Metal-organic frameworks: design and application*. 2010: John Wiley & Sons.
18. Schröder, M., *Functional metal-organic frameworks: gas storage, separation and catalysis*. Vol. 293. 2010: Springer.
19. Rowsell, J.L. and O.M. Yaghi, *Metal–organic frameworks: a new class of porous materials.* Microporous and Mesoporous Materials, 2004. **73**(1): p. 3-14.
20. Eddaoudi, M., et al., *Modular chemistry: secondary building units as a basis for the design of highly porous and robust metal− organic carboxylate frameworks.* Accounts of Chemical Research, 2001. **34**(4): p. 319-330.
21. Nouar, F., et al., *Supermolecular building blocks (SBBs) for the design and synthesis of highly porous metal-organic frameworks.* Journal of the American Chemical Society, 2008. **130**(6): p. 1833-1835.
22. Nugent, P., et al., *Porous materials with optimal adsorption thermodynamics and kinetics for CO^ sub 2^ separation.* Nature, 2013. **495**(7439): p. 80.
23. Eddaoudi, M. and J.F. Eubank, *Insight into the Development of Metal-Organic Materials (MOMs): At Zeolite-Like Metal-Organic Frameworks (ZMOFs).* Metal-Organic Frameworks: Design and Application, 2010: p. 37-89.

24. Desiraju, G.R. and G.W. Parshall, *Crystal engineering: the design of organic solids.* Materials science monographs, 1989. **54**.
25. Scott, H.S., et al., *Novel mode of 2-fold interpenetration observed in a primitive cubic network of formula [Ni(1,2-bis(4-pyridyl)acetylene)$_2$(Cr$_2$O$_7$)]$_n$.* Chemical Communications, 2015. **51**(80): p. 14832-14835.
26. Moulton, B. and M.J. Zaworotko, *From molecules to crystal engineering: supramolecular isomerism and polymorphism in network solids.* Chemical Reviews, 2001. **101**(6): p. 1629-1658.
27. Subramanian, S. and M.J. Zaworotko, *Porous solids by design:[Zn(4,4'-bpy)$_2$(SiF$_6$)]$_n$· xDMF, a single framework octahedral coordination polymer with large square channels.* Angewandte Chemie International Edition, 1995. **34**(19): p. 2127-2129.
28. Uemura, K., et al., *Syntheses, crystal structures and adsorption properties of ultramicroporous coordination polymers constructed from hexafluorosilicate ions and pyrazine.* European Journal of Inorganic Chemistry, 2009. **2009**(16): p. 2329-2337.
29. Kumar, A., et al., *Hybrid ultramicroporous materials (HUMs) with enhanced stability and trace carbon capture performance.* Chemical Communications, 2017. **53**(44): p. 5946-5949.
30. Chen, K.-J., et al., *Benchmark C$_2$H$_2$/CO$_2$ and CO$_2$/C$_2$H$_2$ Separation by Two Closely Related Hybrid Ultramicroporous Materials.* Chem, 2016. **1**(5): p. 753-765.
31. Cui, X., et al., *Pore chemistry and size control in hybrid porous materials for acetylene capture from ethylene.* Science, 2016. **353**(6295): p. 141-144.
32. Mohamed, M.H., et al., *Hybrid Ultra-Microporous Materials for Selective Xenon Adsorption and Separation.* Angewandte Chemie International Edition, 2016. **55**(29): p. 8285-8289.
33. Kumar, A., et al., *Direct air capture of CO$_2$ by physisorbent materials.* Angewandte Chemie International Edition, 2015. **54**(48): p. 14372-14377.

34. Cadiau, A., et al., *A metal-organic framework–based splitter for separating propylene from propane.* Science, 2016. **353**(6295): p. 137-140.
35. Bhatt, P.M., et al., *A fine-tuned fluorinated MOF addresses the needs for trace CO_2 removal and air capture using physisorption.* Journal of the American Chemical Society, 2016. **138**(29): p. 9301-9307.
36. Shekhah, O., et al., *Made-to-order metal-organic frameworks for trace carbon dioxide removal and air capture.* Nature communications, 2014. **5**.
37. Zhang, Z., et al., *Sorting of C_4 olefins with interpenetrated hybrid ultramicroporous materials by combining molecular recognition and size-sieving.* Angewandte Chemie International Edition, 2017.
38. Cadiau, A., et al., *Hydrolytically stable fluorinated metal-organic frameworks for energy-efficient dehydration.* Science, 2017. **356**(6339): p. 731-735.
39. Kumar, A., et al., *Hybrid ultramicroporous materials (HUMs) with enhanced stability and trace carbon capture performance.* Chemical Communications, 2017. **53**(44): p. 5946-5949.
40. Ziaee, A., et al., *Theoretical optimization of pore size and chemistry in SIFSIX-3-M hybrid ultramicroporous materials.* Crystal Growth & Design, 2016. **16**(7): p. 3890-3897.
41. Forrest, K., T. Pham, and B. Space, *Comparing the Mechanism and Energetics of CO_2 Sorption in the SIFSIX Series.* CrystEngComm, 2017.
42. Elsaidi, S.K., et al., *Effect of ring rotation upon gas adsorption in SIFSIX-3-M (M= Fe, Ni) pillared square grid networks.* Chemical Science, 2017. **8**(3): p. 2373-2380.
43. Li, H., et al., *Design and synthesis of an exceptionally stable and highly porous metal-organic framework.* Nature, 1999. **402**(6759): p. 276-279.
44. Zhou, H.-C., J.R. Long, and O.M. Yaghi, *Introduction to metal–organic frameworks*. 2012, ACS Publications.

45. Farha, O.K., et al., *De novo synthesis of a metal–organic framework material featuring ultrahigh surface area and gas storage capacities.* Nature chemistry, 2010. **2**(11): p. 944-948.
46. Furukawa, H., et al., *The chemistry and applications of metal-organic frameworks.* Science, 2013. **341**(6149): p. 1230444.
47. Lee, J., et al., *Metal–organic framework materials as catalysts.* Chemical Society Reviews, 2009. **38**(5): p. 1450-1459.
48. Kuppler, R.J., et al., *Potential applications of metal-organic frameworks.* Coordination Chemistry Reviews, 2009. **253**(23): p. 3042-3066.
49. Eddaoudi, M., et al., *Systematic design of pore size and functionality in isoreticular MOFs and their application in methane storage.* Science, 2002. **295**(5554): p. 469-472.
50. Sagara, T., J. Klassen, and E. Ganz, *Computational study of hydrogen binding by metal-organic framework-5.* The Journal of chemical physics, 2004. **121**(24): p. 12543-12547.
51. Chui, S.S.-Y., et al., *A chemically functionalizable nanoporous material* $[Cu_3(TMA)_2(H2O)_3]_n$. Science, 1999. **283**(5405): p. 1148-1150.
52. Millward, A.R. and O.M. Yaghi, *Metal− organic frameworks with exceptionally high capacity for storage of carbon dioxide at room temperature.* Journal of the American Chemical Society, 2005. **127**(51): p. 17998-17999.
53. Mohamed, M.H., et al., *Pillar substitution modulates* CO_2 *affinity in "mmo" topology networks.* Chemical Communications, 2013. **49**(84): p. 9809-9811.
54. Mohamed, M.H., et al., *Highly selective* CO_2 *uptake in uninodal 6-connected "mmo" nets based upon* MO_4^{2-}*(M= Cr, Mo) pillars.* Journal of the American Chemical Society, 2012. **134**(48): p. 19556-19559.
55. Burd, S.D., et al., *Square Grid and Pillared Square Grid Coordination Polymers–Fertile Ground for Crystal Engineering of Structure and Function.* CHIMIA International Journal for Chemistry, 2013. **67**(6): p. 372-378.

56. Yuan, D., et al., *Stepwise adsorption in a mesoporous metal–organic framework: experimental and computational analysis.* Chemical Communications, 2012. **48**(27): p. 3297-3299.
57. Nugent, P., et al., *Dramatic effect of pore size reduction on the dynamics of hydrogen adsorbed in metal–organic materials.* Journal of Materials Chemistry A, 2014. **2**(34): p. 13884-13891.
58. O'Nolan, D., A. Kumar, and M.J. Zaworotko, *Water Vapor Sorption in Hybrid Pillared Square Grid Materials.* Journal of the American Chemical Society, 2017.
59. Noro, S.i., et al., *A New, Methane Adsorbent, Porous Coordination Polymer [{$CuSiF_6$(4,4'-bipyridine)$_2$}$_n$]*. Angewandte Chemie International Edition, 2000. **39**(12): p. 2081-2084.
60. Forrest, K.A., et al., *Examining the effects of different ring configurations and equatorial fluorine atom positions on CO_2 sorption in [Cu(bpy)$_2$$SiF_6$]*. Crystal Growth & Design, 2013.
61. Elsaidi, S.K., et al., *Hydrophobic pillared square grids for selective removal of CO_2 from simulated flue gas.* Chemical Communications, 2015. **51**(85): p. 15530-15533.
62. Forrest, K.A., et al., *Computational studies of CO_2 sorption and separation in an ultramicroporous metal–organic material.* The Journal of Physical Chemistry C, 2013.
63. Nugent, P., et al., *Enhancement of CO_2 selectivity in a pillared pcu MOM platform through pillar substitution.* Chemical Communications, 2013. **49**(16): p. 1606-1608.
64. Zaworotko, M., et al., *The effect of centred versus offset interpenetration on C_2H_2 sorption in Hybrid Ultramicroporous Materials.* Chemical Communications, 2017.

65. Jorgensen, W.L., D.S. Maxwell, and J. Tirado-Rives, *Development and testing of the OPLS all-atom force field on conformational energetics and properties of organic liquids.* J. Am. Chem. Soc, 1996. **118**(45): p. 11225-11236.
66. Rappé, A.K., et al., *UFF, a full periodic table force field for molecular mechanics and molecular dynamics simulations.* Journal of the American chemical society, 1992. **114**(25): p. 10024-10035.
67. Fang, H., et al., *Recent developments in first-principles force fields for molecules in nanoporous materials.* Journal of Materials Chemistry A, 2014. **2**(2): p. 274-291.
68. Watanabe, T. and D.S. Sholl, *Accelerating applications of metal–organic frameworks for gas adsorption and separation by computational screening of materials.* Langmuir, 2012. **28**(40): p. 14114-14128.
69. Torrisi, A., R.G. Bell, and C. Mellot-Draznieks, *Predicting the impact of functionalized ligands on CO_2 adsorption in MOFs: a combined DFT and grand canonical Monte Carlo study.* Microporous and Mesoporous Materials, 2013. **168**: p. 225-238.
70. Frost, H., T. Düren, and R.Q. Snurr, *Effects of surface area, free volume, and heat of adsorption on hydrogen uptake in metal− organic frameworks.* The Journal of Physical Chemistry B, 2006. **110**(19): p. 9565-9570.
71. Cramer, C.J., *Essentials of computational chemistry: theories and models*. 2013: John Wiley & Sons.
72. Hirao, K., *Multireference Møller—Plesset method.* Chemical physics letters, 1992. **190**(3-4): p. 374-380.
73. Kohn, W. and L.J. Sham, *Self-consistent equations including exchange and correlation effects.* Physical review, 1965. **140**(4A): p. A1133.
74. Odoh, S.O., et al., *Quantum-chemical characterization of the properties and reactivities of metal–organic frameworks.* Chemical reviews, 2015. **115**(12): p. 6051-6111.

75. Perdew, J.P., K. Burke, and M. Ernzerhof, *Generalized gradient approximation made simple.* Physical review letters, 1996. **77**(18): p. 3865.
76. Becke, A.D., *Density-functional exchange-energy approximation with correct asymptotic behavior.* Physical review A, 1988. **38**(6): p. 3098.
77. Lee, C., W. Yang, and R.G. Parr, *Development of the Colle-Salvetti correlation-energy formula into a functional of the electron density.* Physical review B, 1988. **37**(2): p. 785.
78. Tao, J., et al., *Climbing the density functional ladder: Nonempirical meta–generalized gradient approximation designed for molecules and solids.* Physical Review Letters, 2003. **91**(14): p. 146401.
79. Luo, S., et al., *Density functional theory of open-shell systems. the 3d-series transition-metal atoms and their cations.* Journal of chemical theory and computation, 2013. **10**(1): p. 102-121.
80. Becke, A.D., *Phys. Re V. A 1988, 38, 3098.(b) Becke.* J. Chem. Phys, 1993. **98**: p. 5648.
81. Adamo, C. and V. Barone, *Toward reliable density functional methods without adjustable parameters: The PBE0 model.* The Journal of chemical physics, 1999. **110**(13): p. 6158-6170.
82. Grimme, S., *Density functional theory with London dispersion corrections.* Wiley Interdisciplinary Reviews: Computational Molecular Science, 2011. **1**(2): p. 211-228.
83. Grimme, S., *Semiempirical GGA-type density functional constructed with a long-range dispersion correction.* Journal of computational chemistry, 2006. **27**(15): p. 1787-1799.
84. Grimme, S., S. Ehrlich, and L. Goerigk, *Effect of the damping function in dispersion corrected density functional theory.* Journal of computational chemistry, 2011. **32**(7): p. 1456-1465.
85. Gao, J. and M.A. Thompson, *Combined quantum mechanical and molecular mechanical methods*. 1998: ACS Publications.

86. Kresse, G. and J. Furthmüller, *Efficiency of ab-initio total energy calculations for metals and semiconductors using a plane-wave basis set.* Computational materials science, 1996. **6**(1): p. 15-50.
87. Kresse, G. and J. Furthmüller, *Efficient iterative schemes for ab initio total-energy calculations using a plane-wave basis set.* Physical review B, 1996. **54**(16): p. 11169.
88. Valenzano, L., et al., *Structure–activity relationships of simple molecules adsorbed on CPO-27-Ni metal–organic framework: In situ experiments vs. theory.* Catalysis today, 2012. **182**(1): p. 67-79.
89. Kresse, G. and D. Joubert, *From ultrasoft pseudopotentials to the projector augmented-wave method.* Physical Review B, 1999. **59**(3): p. 1758.
90. Goedecker, S., M. Teter, and J. Hutter, *Separable dual-space Gaussian pseudopotentials.* Physical Review B, 1996. **54**(3): p. 1703.
91. Pham, T., et al., *Theoretical investigations of CO_2 and H_2 sorption in an interpenetrated square-pillared metal–organic material.* The Journal of Physical Chemistry C, 2013.
92. Mayo, S.L., B.D. Olafson, and W.A. Goddard, *DREIDING: a generic force field for molecular simulations.* Journal of Physical chemistry, 1990. **94**(26): p. 8897-8909.
93. Siderius, D.W. and V.K. Shen, *Use of the grand canonical transition-matrix Monte Carlo method to model gas adsorption in porous materials.* The Journal of Physical Chemistry C, 2013. **117**(11): p. 5861-5872.
94. Mones, L., et al., *The adaptive buffered force QM/MM method in the CP2K and AMBER software packages.* Journal of computational chemistry, 2015. **36**(9): p. 633-648.
95. VandeVondele, J., et al., *Quickstep: Fast and accurate density functional calculations using a mixed Gaussian and plane waves approach.* Computer Physics Communications, 2005. **167**(2): p. 103-128.

96. CP2k, A., *General Program to Perform Molecular Dynamics Simulations.* CP2k developers group under the terms of the GNU General Public License.
97. VandeVondele, J. and J. Hutter, *Gaussian basis sets for accurate calculations on molecular systems in gas and condensed phases.* The Journal of chemical physics, 2007. **127**(11): p. 114105.
98. Campañá, C., B. Mussard, and T.K. Woo, *Electrostatic Potential Derived Atomic Charges for Periodic Systems Using a Modified Error Functional.* Journal of Chemical Theory and Computation, 2009. **5**(10): p. 2866-2878.
99. Belof, J. and B. Space, *Massively Parallel Monte Carlo (MPMC).* Available on Google Code, 2012.
100. Metropolis, N., et al., *Equation of state calculations by fast computing machines.* The journal of chemical physics, 1953. **21**(6): p. 1087-1092.
101. Mullen, A.L., et al., *A polarizable and transferable PHAST CO_2 potential for materials simulation.* Journal of chemical theory and computation, 2013. **9**(12): p. 5421-5429.
102. McQuarrie, D., *Statistical Mechanics. 2000.* Sausalito, Calif.: University Science Books, 2004. **12**: p. 641.
103. Frenkel, D. and B. Smit, *Understanding molecular simulation: From algorithms to applications*. 2002, Elsevier (formerly published by Academic Press). p. 1-638.
104. Peng, D.-Y. and D.B. Robinson, *A new two-constant equation of state.* Industrial & Engineering Chemistry Fundamentals, 1976. **15**(1): p. 59-64.
105. Jones, J.E. *On the determination of molecular fields. II. From the equation of state of a gas*. in *Proceedings of the Royal Society of London A: Mathematical, Physical and Engineering Sciences*. 1924. The Royal Society.
106. Ewald, P.P., *Die Berechnung optischer und elektrostatischer Gitterpotentiale.* Annalen der Physik, 1921. **369**(3): p. 253-287.
107. Wells, B.A. and A.L. Chaffee, *Ewald summation for molecular simulations.* Journal of chemical theory and computation, 2015. **11**(8): p. 3684-3695.

108. Van Duijnen, P.T. and M. Swart, *Molecular and atomic polarizabilities: Thole's model revisited.* The Journal of Physical Chemistry A, 1998. **102**(14): p. 2399-2407.

109. Applequist, J., J.R. Carl, and K.-K. Fung, *Atom dipole interaction model for molecular polarizability. Application to polyatomic molecules and determination of atom polarizabilities.* Journal of the American Chemical Society, 1972. **94**(9): p. 2952-2960.

110. Bode, K.A. and J. Applequist, *A new optimization of atom polarizabilities in halomethanes, aldehydes, ketones, and amides by way of the atom dipole interaction model.* The Journal of Physical Chemistry, 1996. **100**(45): p. 17820-17824.

111. Thole, B.T., *Molecular polarizabilities calculated with a modified dipole interaction.* Chemical Physics, 1981. **59**(3): p. 341-350.

112. McLaughlin, K., et al., *Efficient calculation of many-body induced electrostatics in molecular systems.* The Journal of chemical physics, 2013. **139**(18): p. 184112.

113. Allen, M.P. and M.R. Wilson, *Computer simulation of liquid crystals.* Journal of computer-aided molecular design, 1989. **3**(4): p. 335-353.

114. Nicholson, D., *Computer simulation and the statistical mechanics of adsorption*. 1982: Academic Press.

Appendix

Paper Under Review (see following pages)